From Quanteye to Iqueye and beyond:

the road to Quantum Astronomy

Cesare Barbieri

University of Padova, Italy

cesare.barbieri@unipd.it

Summary - 1

I'll describe our experiments for very high time and space resolution:

1 –time: we have conceived a photometer capable to time tag the arrival time of each photon with a resolution and accuracy of **few hundred picoseconds**, for hours of continuous acquisition and with a dynamic range of more than 6 orders of magnitude. The final goal is a 'quantum' photometer for the E-ELT capable to detect and measure **second order correlation effects** (according to Glauber's description of the EM field) in the photon stream from celestial sources.

2 - Among the second order effects, **Hanbury Brown - Twiss Intensity Interferometry** has been already successfully tested at the NTT, giving hopes to perform very high spatial resolution observations **among telescopes not optically linked**, e.g. the E-ELT at Cerro Armazones and the VLT at Cerro Paranal, or Cerenkov light telescopes such as Magic or CTA.

Two prototype units have been built and operated, one for the Asiago 1.8m telescope (Aqueye) and one for the 3.5m NTT (Iqueye).

Results will be presented.

the roots of Queye and Iqueye

OWL Instrument Concept Study

QuantEYE
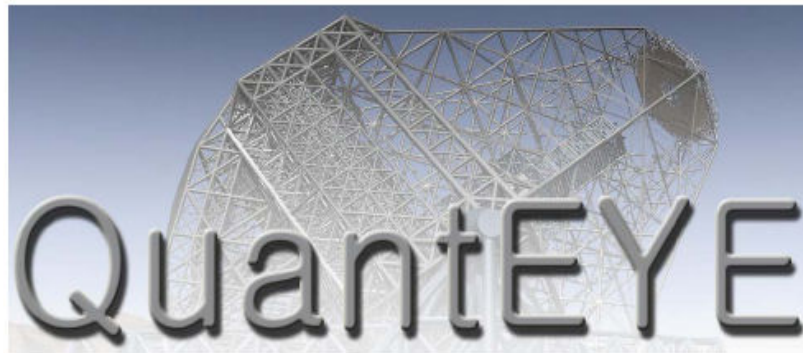
QUANTUM OPTICS INSTRUMENTATION FOR ASTRONOMY

D. Dravins [1], C. Barbieri [2],

V. Da Deppo [3], D. Faria [1], S. Fornasier [2],

R. A. E. Fosbury [4], L. Lindegren [1], G. Naletto [3], R. Nilsson [1],

T. Occhipinti [3], F. Tamburini [2], H. Uthas [1], L. Zampieri [5]

(1) Lund Observatory, Box 43, SE-22100 Lund, Sweden
(2) Department of Astronomy, University of Padova, Vicolo dell'Osservatorio 2, IT-35122 Padova, Italy
(3) Dept. of Information Engineering, University of Padova, Via Gradenigo, 6/B, IT-35131 Padova, Italy
(4) Space Telescope-European Coordinating Facility & European Southern Observatory, Karl-Schwarzschild-Straße 2, DE-85748 Garching bei München, Germany
(5) INAF – Astronomical Observatory of Padova, Vicolo dell'Osservatorio 5, IT-35122 Padova, Italy

LUND UNIVERSITY

OWL-CSR-ESO-00000-0162

In Sept. 2005, we completed a study (QuantEYE, the ESO Quantum Eye) in the frame of the studies for the (then) 100m Overwhelmingly Large (OWL) telescope.

The main goal of the study was to demonstrate the possibility to reach the picosecond time resolution (Heisenberg limit) needed to bring quantum optics concepts into the astronomical domain, with two main scientific aims in mind:
- *Measure the entropy of the light beam through the statistics of the photon arrival time*
- *Demonstrate the feasibility of astronomical photon correlation spectroscopy and of a modern version of the Hanbury Brown Twiss Intensity Interferometry*

Second Order Correlation Function

$$g^{(2)}_{d}(\tau) = \frac{\langle I(r_1,t_1) I(r_2,t_2) \rangle}{\langle I(r_1,t_1) \rangle \langle I(r_2,t_2) \rangle}$$

(R. Glauber, 1965, Nobel Prize 2005)

with $r_2 - r_1 = d$ and $t_2 - t_1 = \tau$

1 - If $\tau \neq 0$ and d=0 one gets photon correlation spectroscopy (R = 10^9- 10^{10} necessary to resolve *lased* spectral lines) .

2 - If τ=0 and $d \neq 0$ one gets Hanbury Brown - Twiss Intensity Inteferometry (Narrabri) .

Why Extremely Large Telescopes?

The above mentioned quantum correlations are fully developed on time scales of the order of the *inverse optical bandwidth*. For instance, with the very narrow band pass of 1 A (0.1 nm) in the visible, through a definite polarization state, typical time scales are $\approx 10^{-11}$ seconds (10 picoseconds).

However, the photon flux is very weak even from bright stars, so that only Extremely Large Telescopes (ELTs) can bring Quantum Optical effects in the astronomical reaches.

Telescope diameter	Intensity $\langle I \rangle$	Second-order correlation $\langle I^2 \rangle$
3.6 m	1	1
8.2 m	5	27
4 × 8.2 m	21	430
50 m	193	37,000

The amplitude of second order functions increases with the square of the telescope area (not diameter!), so that a 40m telescope will be 256 times more sensitive to such correlations than the existing 8-10m telescopes.

The HBT Intensity Interferometer (HBTII)

The correlation or *intensity* interferometer was invented around 1954 by R. Hanbury Brown and R. Q. Twiss.

A large stellar interferometer was completed in 1965 at Narrabri, Australia, and by the end of the decade it had measured the angular diameters of more than 30 stars, including Main Sequence blue stars.

The light-gathering power of the 6.5 m diameter mirrors, the detectors (photomultipliers), analog electronics etc. allowed the Narrabri interferometer to operate down to magnitude +2.0, a fairly bright limit indeed.

The intrinsically low efficiency of the system made the HBTII essentially forgotten, in favor of Michelson type (amplitude and phase) interferometers, e.g. the ESO VLTI.
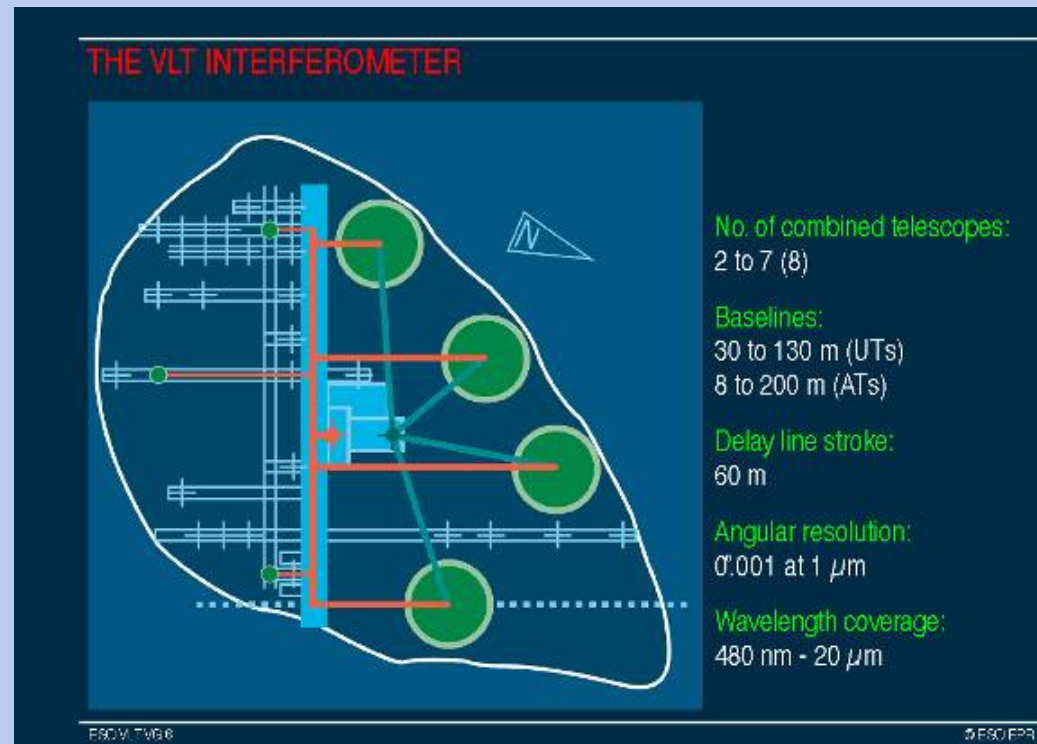
Future of HBTII with E-ELT?

• Quite recently, HBTII has been resurrected for a variety of reasons:

• ease of adjusting the time delays of the channels to equality within few centimeters (***electronic instead of optical*** path compensation);

• immunity to seeing: ***adaptive optics is not required;***

• ***blue sensitivity,*** with the possibility to utilize the large body of data obtained in the Near-IR from Michelson-type interferometers and to supplement their data with observations in this spectral region**;**

• ***Main Sequence blue stars can be reached***, and not only the red Giants and SuperGiants commonly studied with Michelson interferometers.

Very Long Baseline Optical Interferometry

A further advantage of HBTII is that ***no optical link is needed***: it can be performed with *two distant* telescopes not in direct view. Only time tagging to better than say 1ns and proper account of atmospheric refraction and delays. The concept is currently being tested by D. Dravins and collaborators with VERITAS Cherenkov light telescopes in Arizona.

With little effort it could be tested also with two telescopes of the ESO VLT.

THE VLT INTERFEROMETER

No. of combined telescopes:
2 to 7 (8)

Baselines:
30 to 130 m (UTs)
8 to 200 m (ATs)

Delay line stroke:
60 m

Angular resolution:
0".001 at 1 μm

Wavelength coverage:
480 nm - 20 μm

From theory to reality: the key technological limitation is the detector

The most critical point, and driver for the design of Quanteye and our prototypes, was the selection of very fast, efficient and accurate photon counting detectors.

No detector on the market had all needed capabilities .

In order to proceed, we choose ***SPADs operating in Geiger mode***. They give ≈35 ps time resolution with count rates as high as 15 MHz, and a fair QE. The main drawback of SPADs was the lack of CCD-like arrays.

To overcome both the SPAD limitations and the difficulties of a reasonable optical design (coupling the pupil of large telescope to a single 50 - 100 μm detector), we decided to ***split the problem***: we designed QuantEYE by subdividing the pupil into *10 × 10* sub-pupils, each of them focused on a single SPAD, giving a total of *100 distributed* SPAD's. In such a way, a "sparse" SPAD array ***collecting all light and coping with the required very high count rate*** could be obtained. The distributes array samples the telescope pupil, so that a system of *100* parallel smaller telescopes is realized, ***each one acting as a fast photometer.***

Fosbury

AquEYE

The Quanteye concepts was tested with a much smaller version of the instrument, named AquEYE, the Asiago Quantum Eye.
It is mounted on the AFOSC camera of the Asiago-Cima Ekar (Italy) 182 cm telescope (AFOSC plays the role of a 1:3 focal reducer).

MPD's SPADs

The selected detectors are Geiger mode SPADs produced by MPD (Italy). They are operated in continuous mode, the timing circuit and cooling stage are integrated in a ruggedized box. The timing accuracy out of the NIM connector is around **35 ps**.

Their main drawbacks are the small sensitive area (50 – 100 μm diameter), a ≈77 ns dead time and a 1.5% afterpulsing probability.

Measured at Catania Observatory
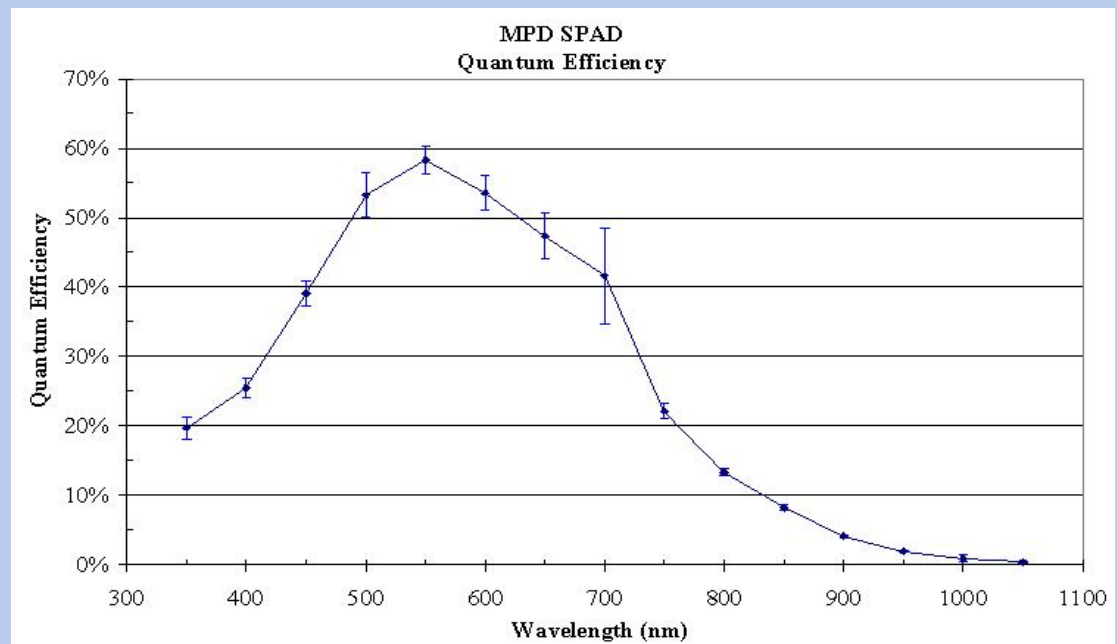
AquEYE optomechanical design

The light beam from AFOSC is divided in **four parts** by means of a pyramidal mirror. Each beam is then focused on its own SPAD by another 1:3 focal reducer made by a pair of doublets.

pinhole

pyramid

1:3 focal reducer

SPAD

SPAD

filter

pyramid
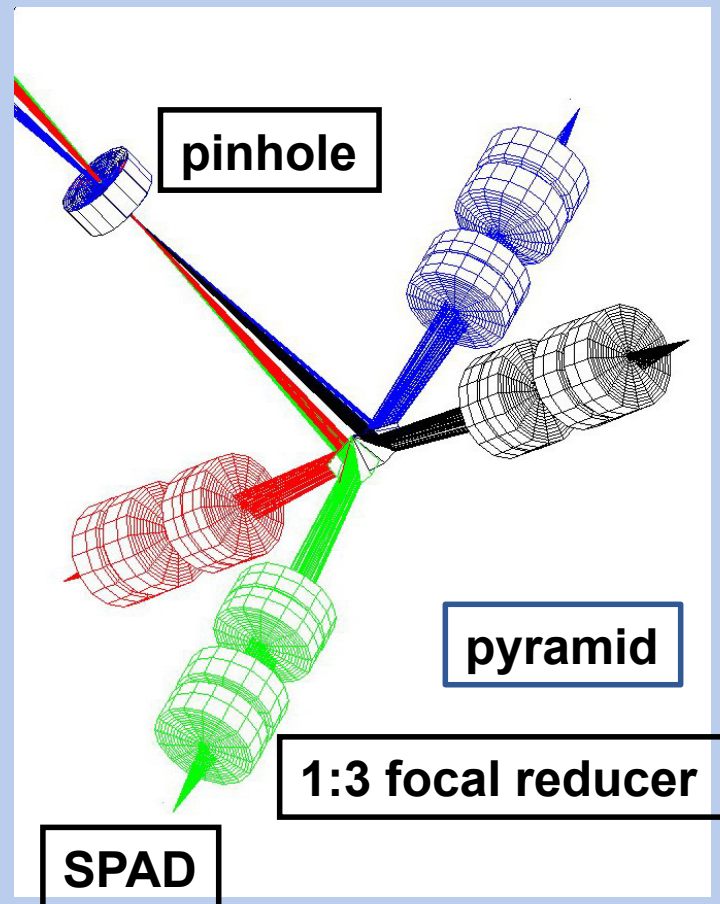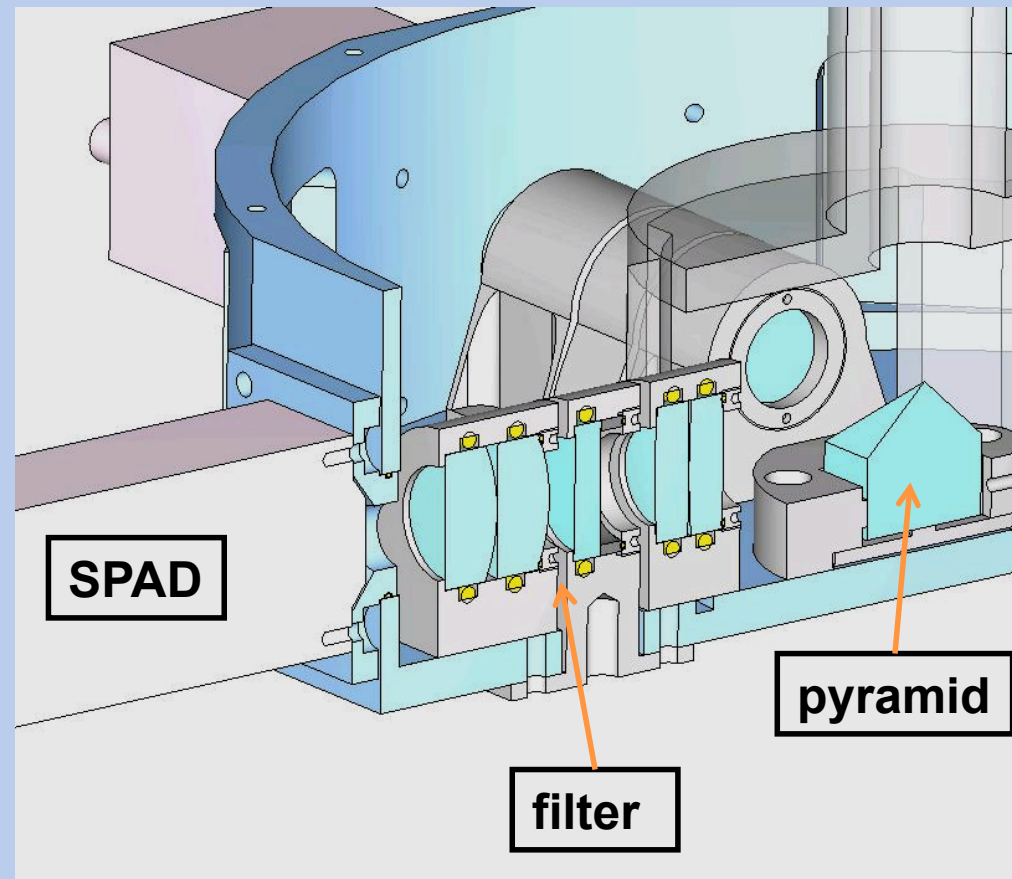
Advantages of multiple pupils

1 - In conjunction with the pupil splitting concept, by separately recording the counts, multiple detectors give the possibility of **simultaneous multicolor photometry** and to perform **cross correlation of the 4 sub-apertures (HBTII experiment)**.

2 – when summing together the 4 outputs, we obtain a **partial recovery of the dead time**.
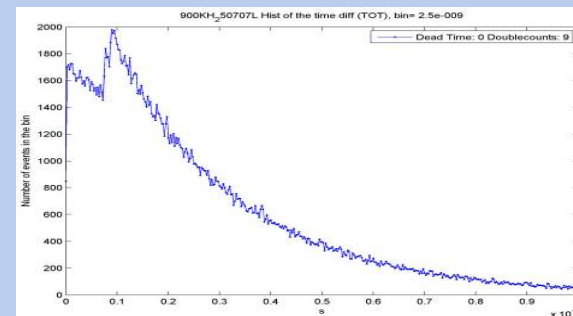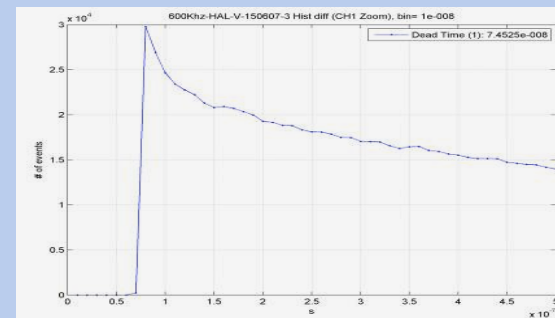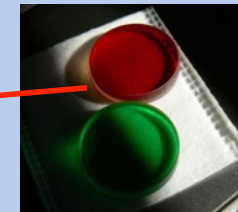
AquEYE Optomechanics
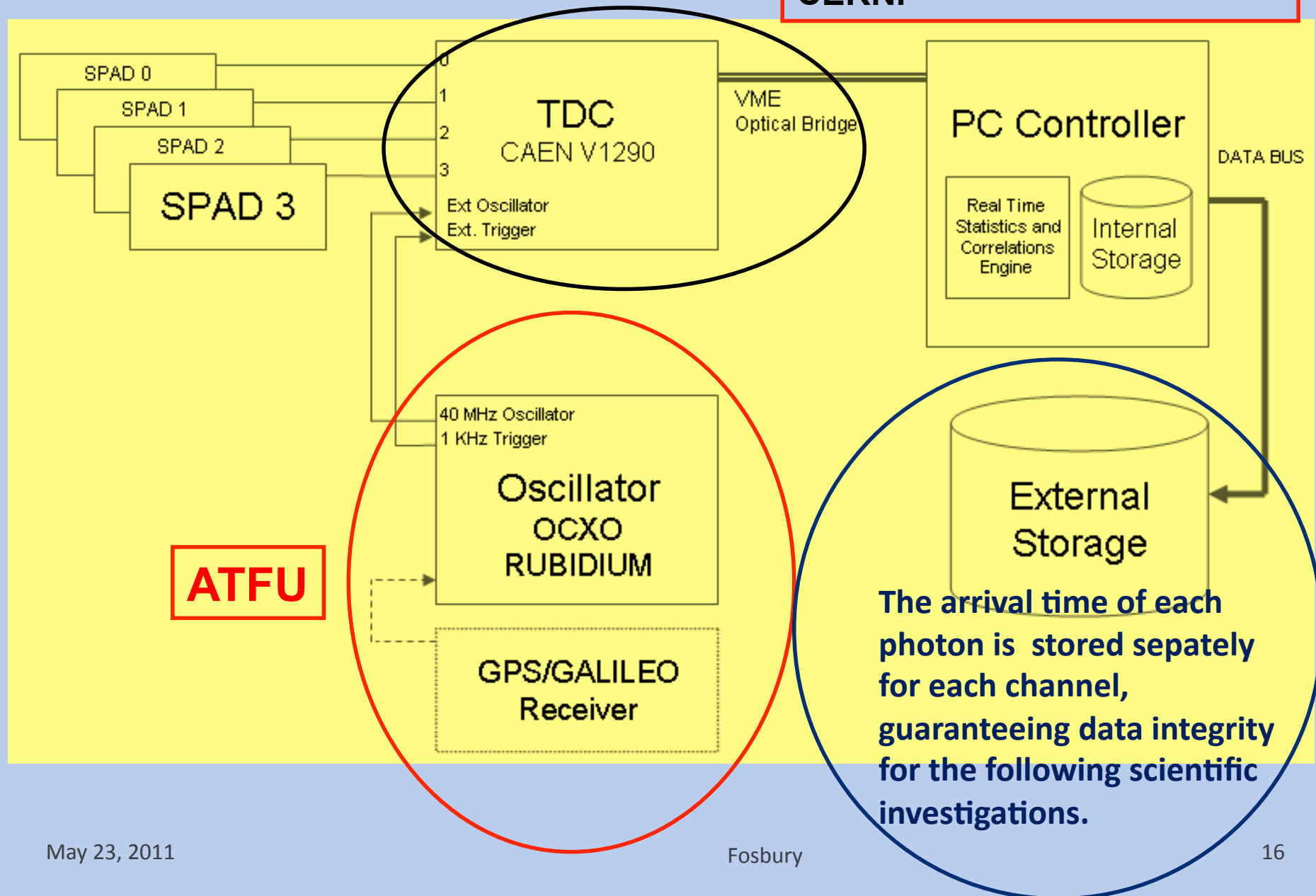

AFOSC focus
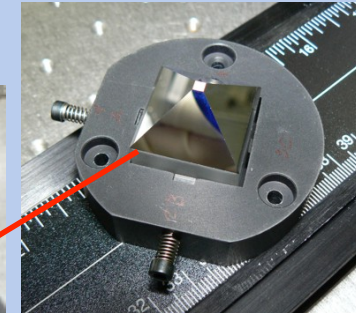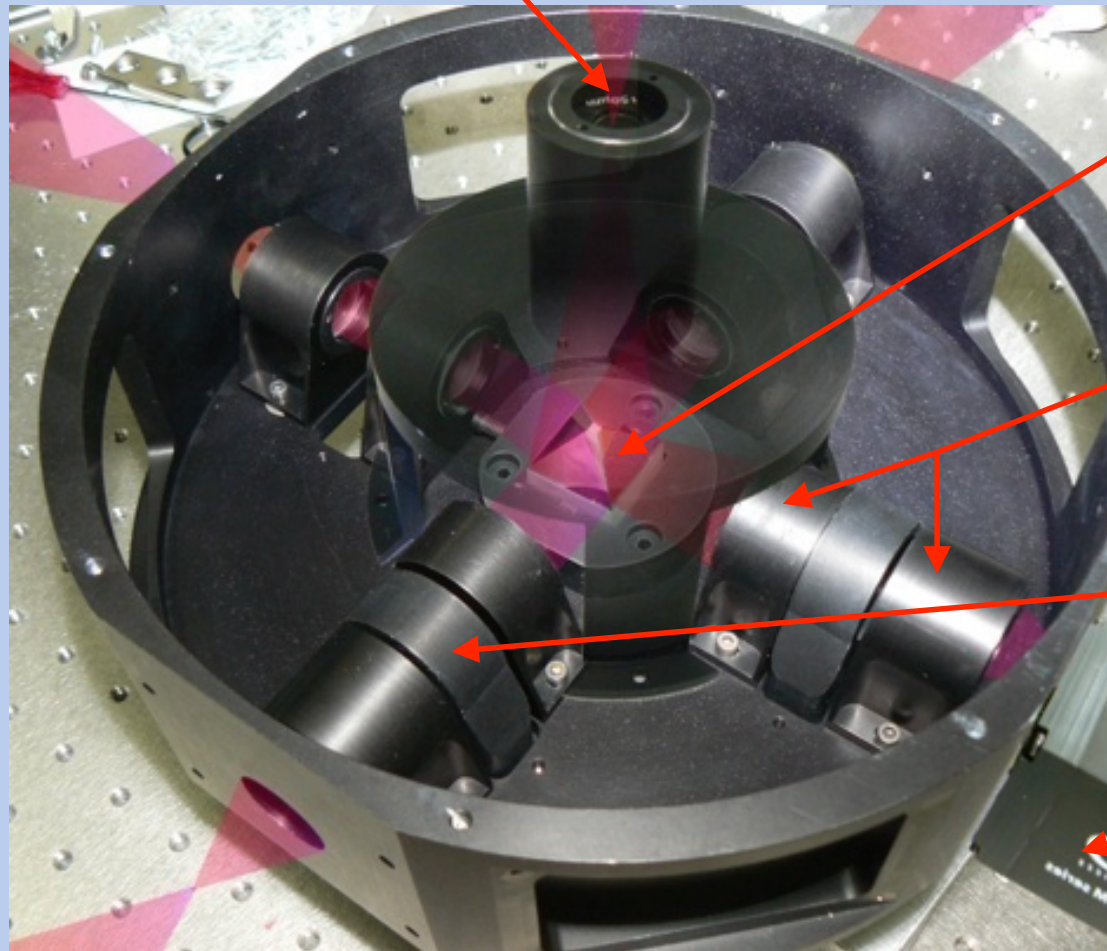
Pyramid
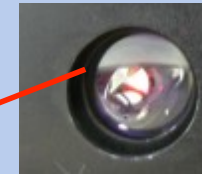
Focusing lenses

Filters

SPAD

AquEYE Electronics

SPAD 0
SPAD 1
SPAD 2
SPAD 3

0
1
2
3

TDC
CAEN V1290

Ext Oscillator
Ext. Trigger

VME
Optical Bridge

PC Controller

DATA BUS

Real Time Statistics and Correlations Engine

Internal Storage

40 MHz Oscillator
1 KHz Trigger

Oscillator
OCXO
RUBIDIUM

GPS/GALILEO
Receiver

ATFU

External Storage

The arrival time of each photon is stored sepately for each channel, guaranteeing data integrity for the following scientific investigations.

Acquisition and Time System

10 MHz Sinusoidal

40 MHz TTL

SRS FS725 Rubidium Frequency Standard
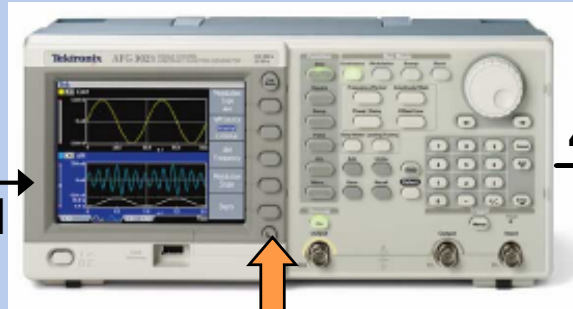
Tektronix AFG3251 Signal Generator
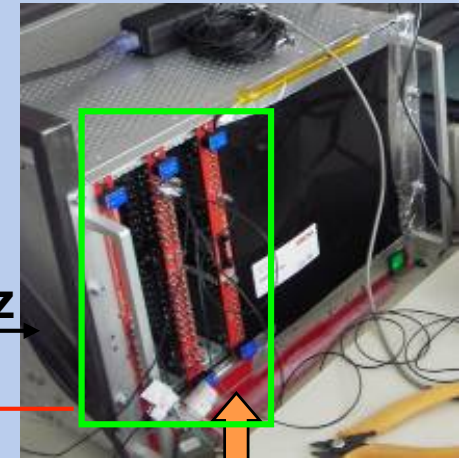
CAEN VME CRATE with V2718, V976 and V1290N

J1 - power and I/O connector

J2 - 10 MHz connector

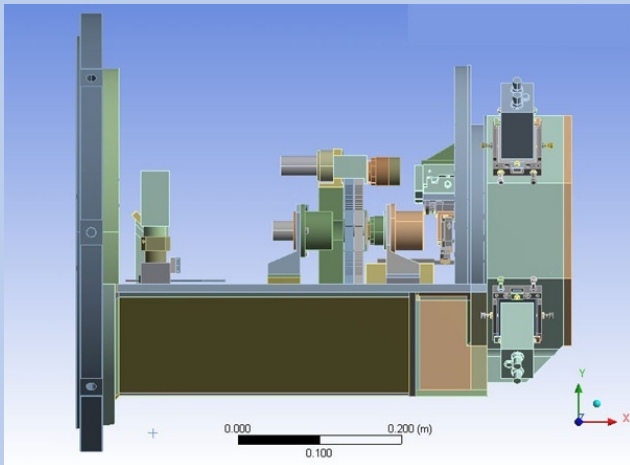J3 - 1 PPS connector

J4 - Antenna interface
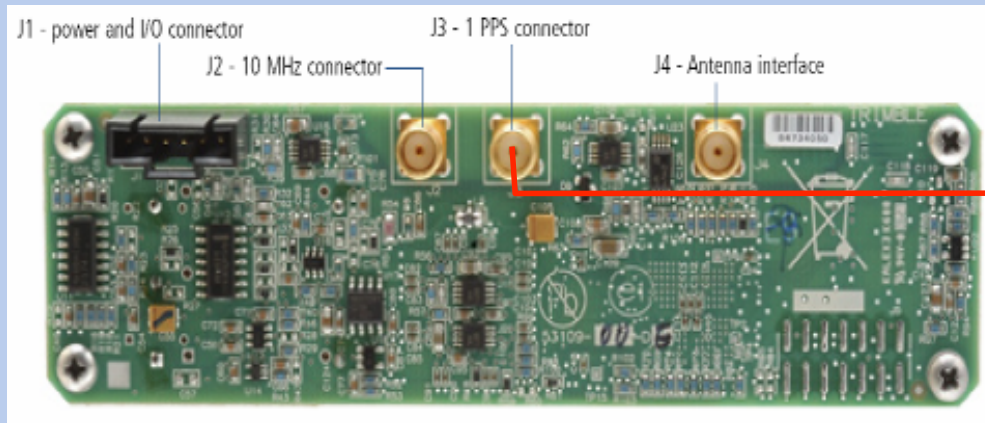
1 PPS TTL

1 PPS NIM

GPS receiver
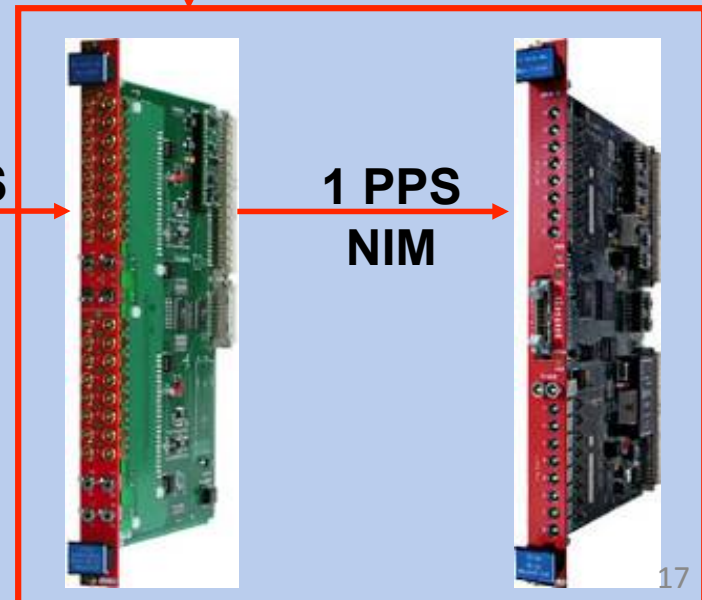
From Asiago to La Silla

Thanks to the positive experience of AquEYE, it was decided to realize IquEYE, a more complex instrument for applications to a larger telescope, namely the ESO 3.5m NTT in La Silla (Chile). The same basic optical solution of pupil splitting in 4 was maintained.

The main modification was the utilization of a new production batch of MPD SPADs, with **100 micrometer effective area diameter, lower dark counts and better engineering**.
After a first run in Jan 2009, some improvements were introduced in Dec. 2010.

Iqueye

A fiber fed fifth spad on the NTT focal plane to measure the sky brightness
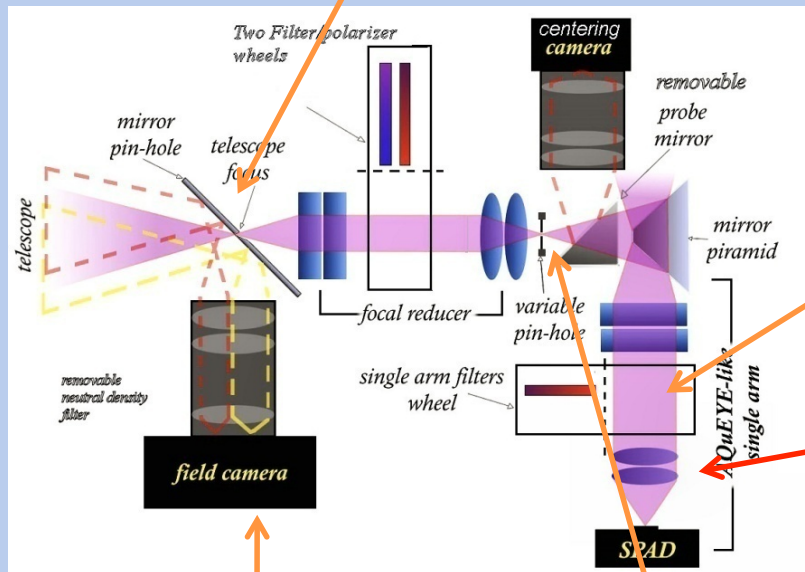
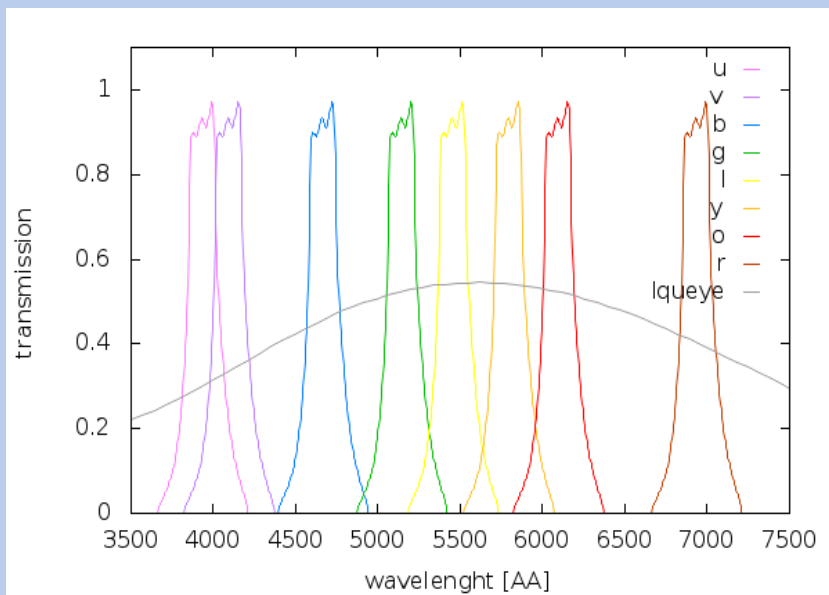**Filter wheel in each SPAD: simultaneous multicolour photometry**

Custom made lenses for better light concentration on the SPAD (more than 99.9%)

Improved entrance pinhole and viewing camera

Control of back-scattered light

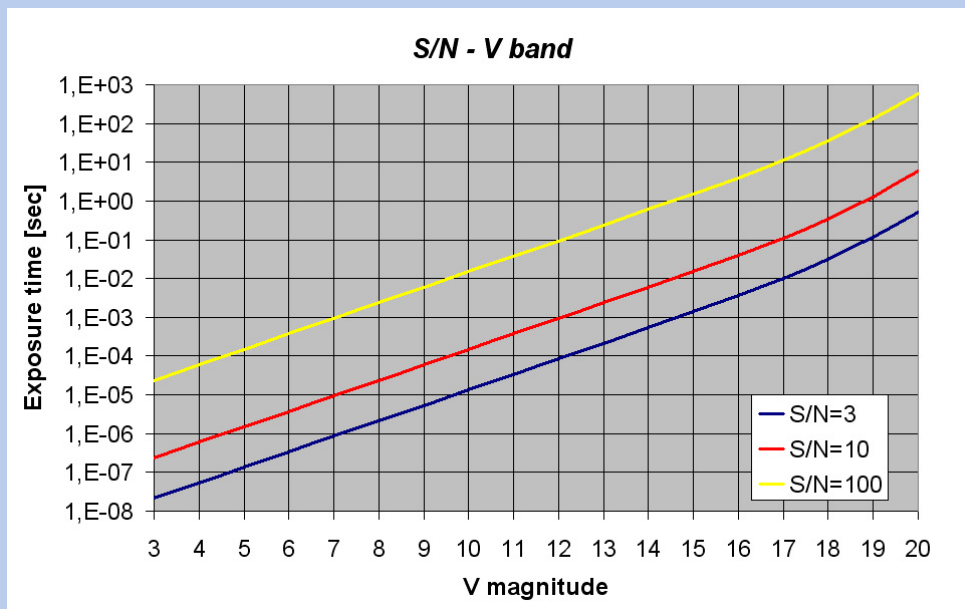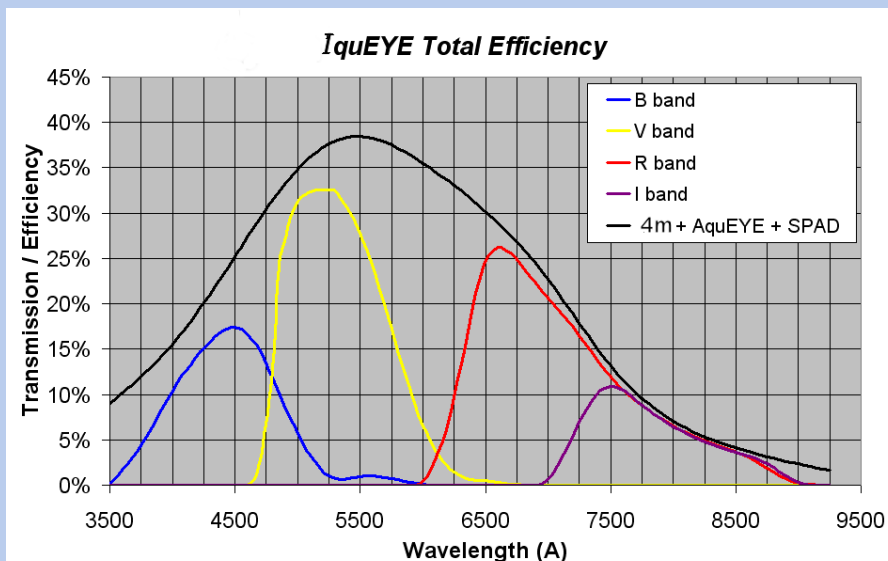**Hardware and software for data acquistion and control have been streamlined.**
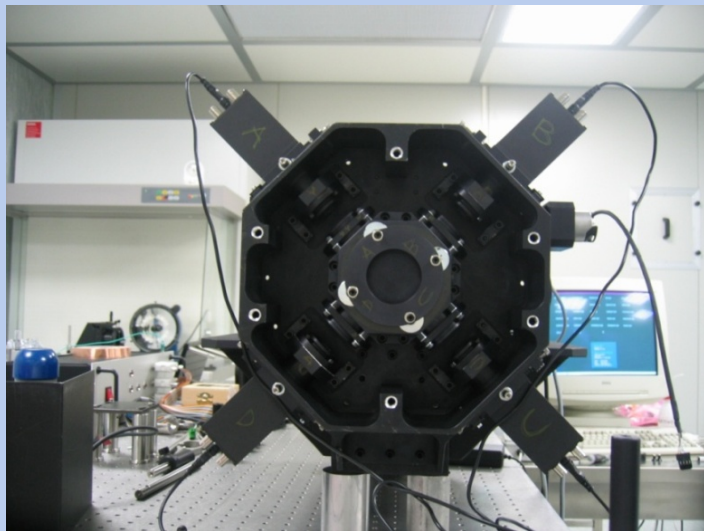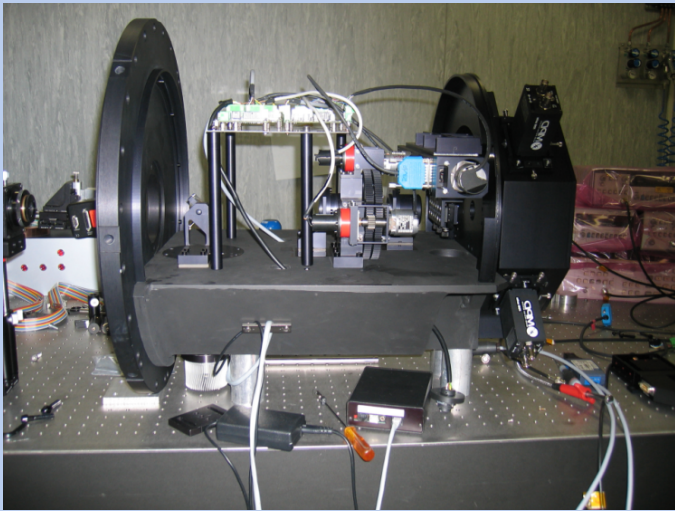
Response of Iqueye

Broadband filters FWHM=100nm, central wavelenghts 450,550,650 nm

Intermediate filters, FWHM=10nm, central wavelengths: 394, 410, 467, 515, 546, 580, 610, 694 nm.

Narrow band filters: Hα (656/3 nm), O [III] (501/1 nm), He II (468/2 nm), O I(630/2 nm).

Photos of Iqueye

# Some results on optical pulsars

Timing of
the CRAB pulsar

Main actors:

C. Barbieri, G. Naletto, L. Zampieri, M. Calvani, C. Germanà,
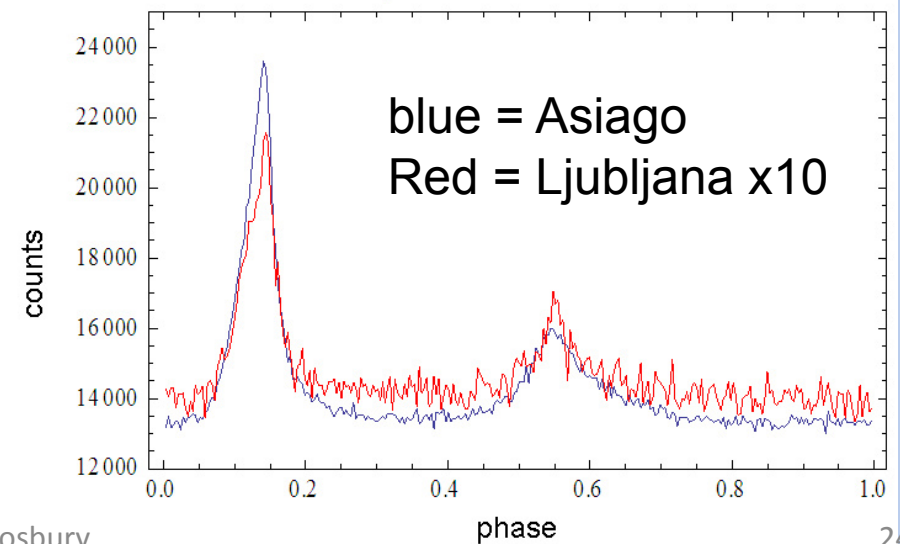E. Verroi, P. Zoccarato,T. Occhipinti, I. Capraro, G. Codogno

A. Čadež, M. Barbieri, A. Possenti, A. Patruno, A. Shearer

Asiago Oct 2008

in Oct. 2008, simultaneous data were taken with the Ljubljana Observatory with a common reference system provided by a GPS and GALILEO-GNSS receiver
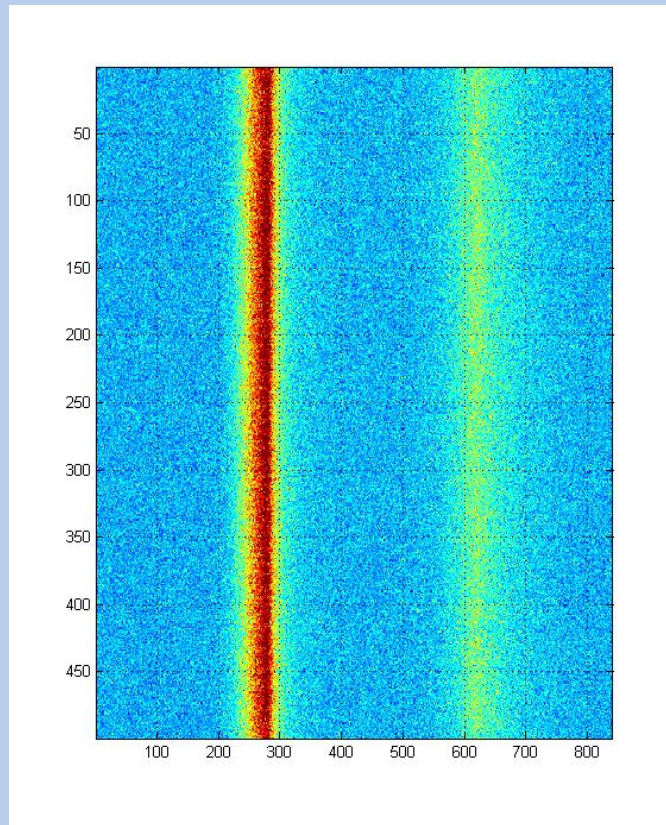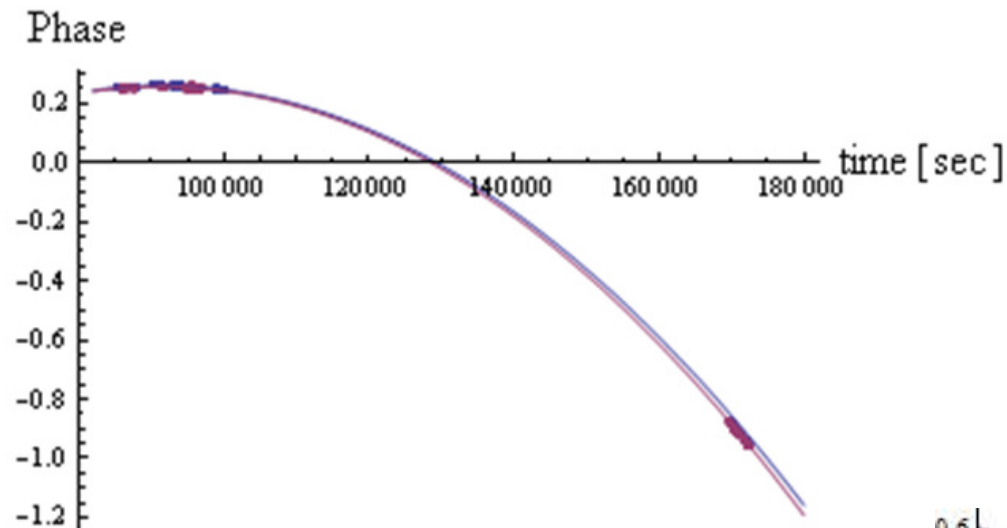

Waterfall diagram
Asiago data

blue = Asiago
Red = Ljubljana x10

Excellent co-phasing - 1

of the optical data(Asiago vs. Ljubljana) over several days of joint observations, *to our knowledge the first experiment of such sort*
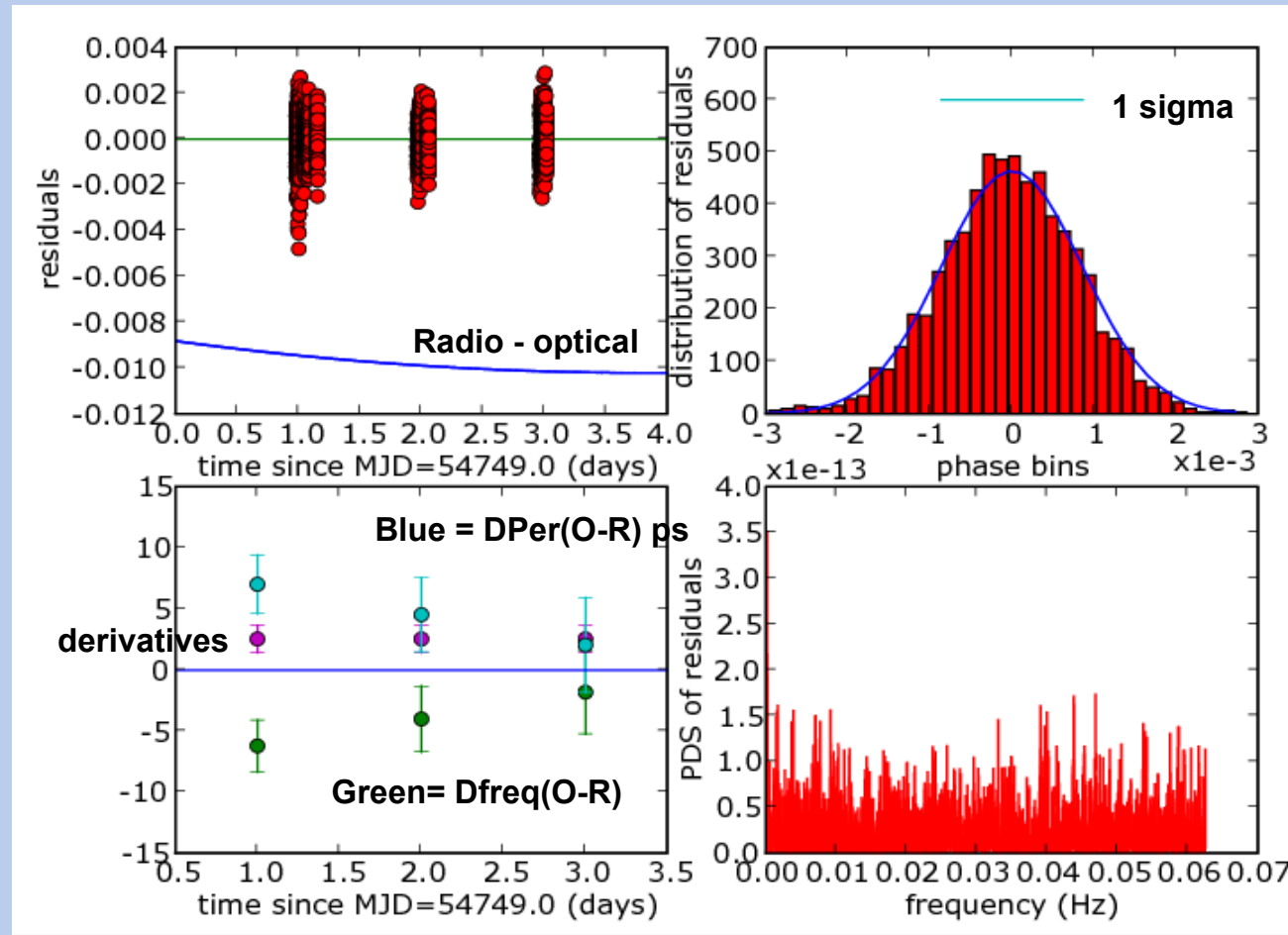

**Just for fun: distance Asiago – Ljubljana
(Copernicus – Vega)
Cartesian distance: 230. 4 km
Google Earth: 230.2 Km
From phase residuals: 229.2 Km
(preliminary, to be refined)**
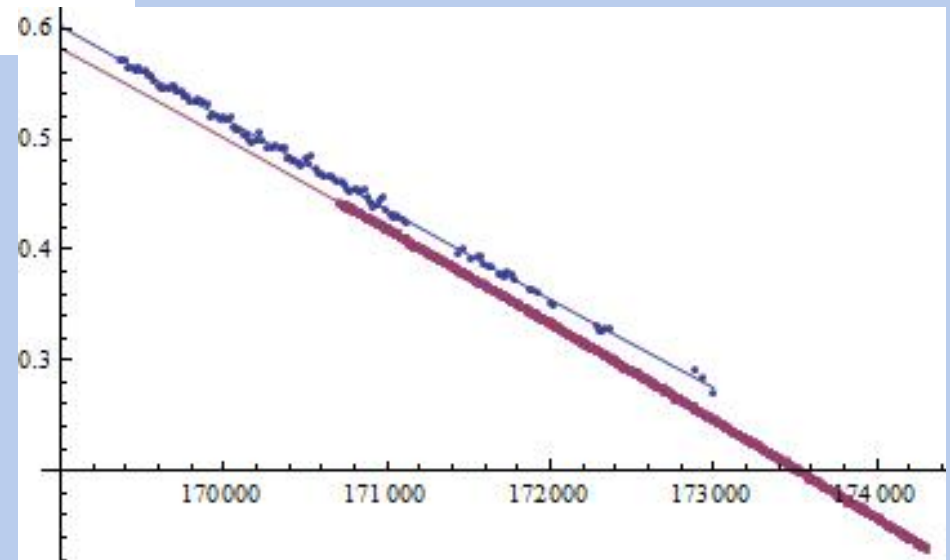
Excellent co-phasing - 2

2 - of the optical vs radio (Jodrell Bank) *average* ephemeris

**Asiago periods = Jodrell Bank periods to better than few picoseconds.**

Phase residuals: smaller than 1 milliphase.

At the NTT - 2009

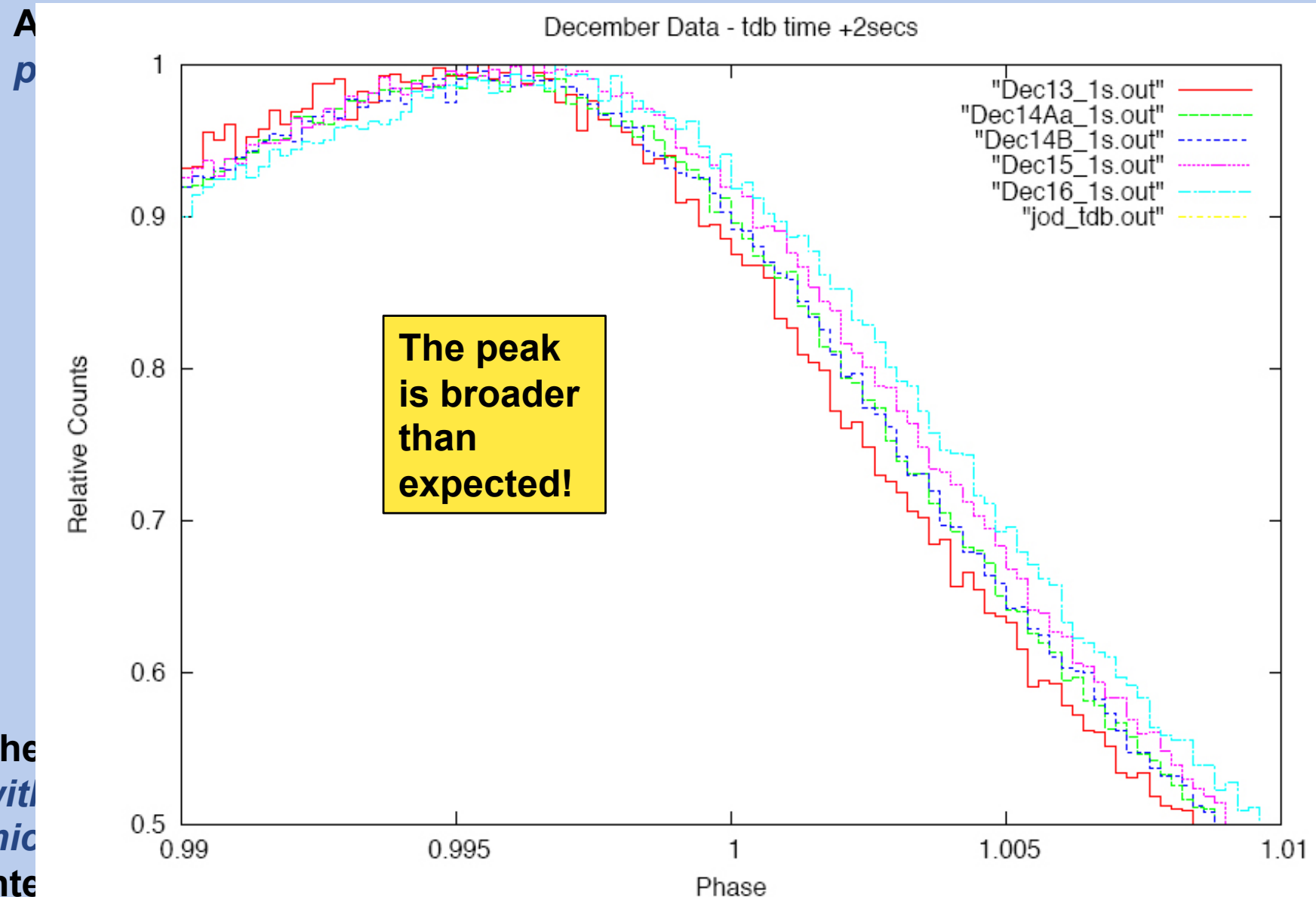**The Crab pulsar was observed in January 2009 and again in December 2009.**

In the last occasion simultaneous data were obtained with Jodrell Bank, which detected about 40 Giant Radio Bursts during the Iqueye observations.

The CRAB pulsar at the NTT

3 μs bin width – all data

3microsec = 10^{-4} P

Relative Counts

Phase, radio peak at phase 0
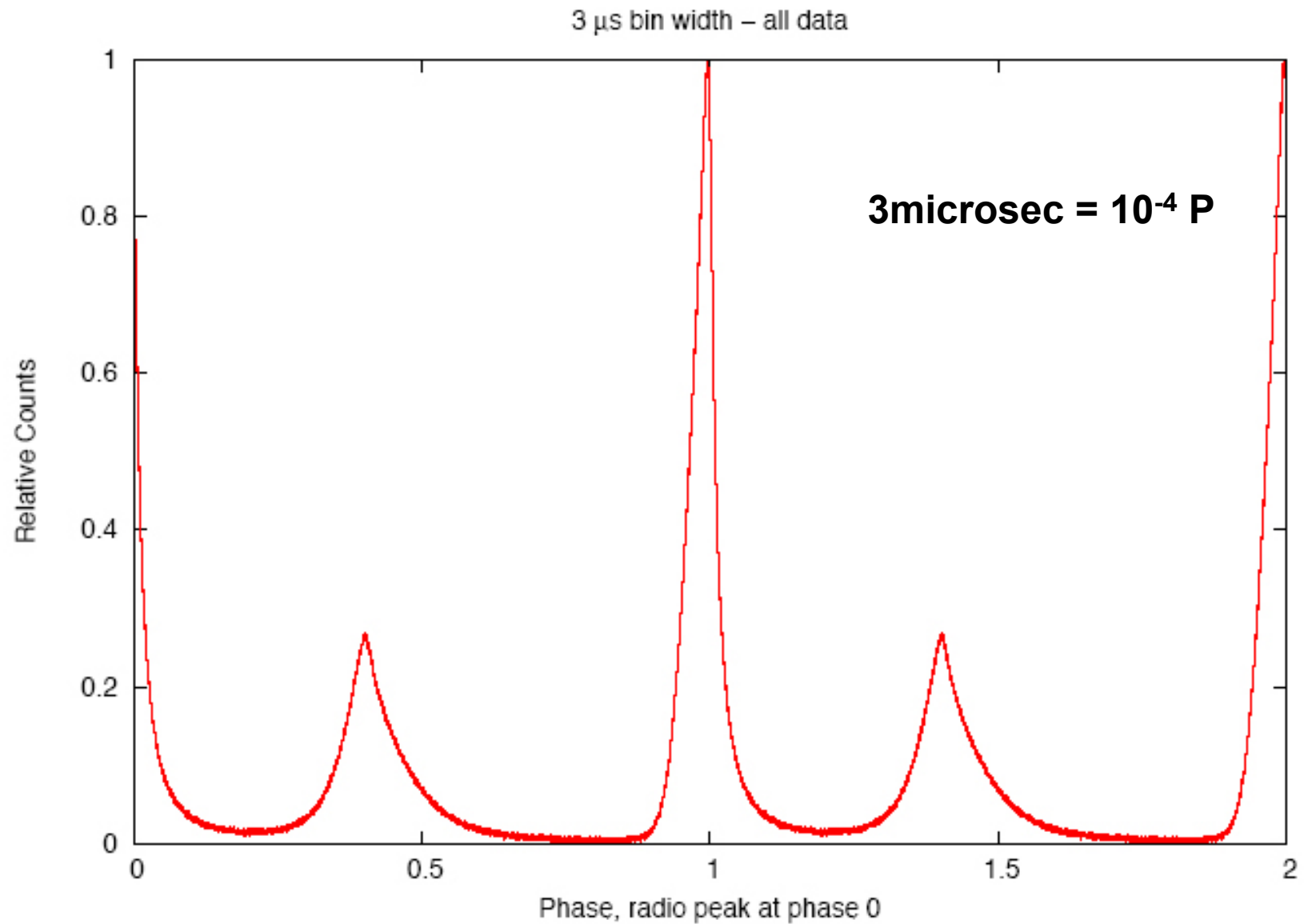
Accuracy of period and phase difference

Some conclusions from Crab pulsar

Iqueye at the NTT provides the best timing of photon arrival times of all optical instruments. In a few hours we reproduce to the picosecond level the JB ephemerides *averaged over decades*.

We are analyzing the arrival times of the Giant Radio Bursts, in order to correlate radio and optical.

Barycentering is trickier than expected. The barycenter of the Solar System is probably not defined to better than 10 nanoseconds or so.

Atmospheric delay models for visible light are desirable and are being implemented.
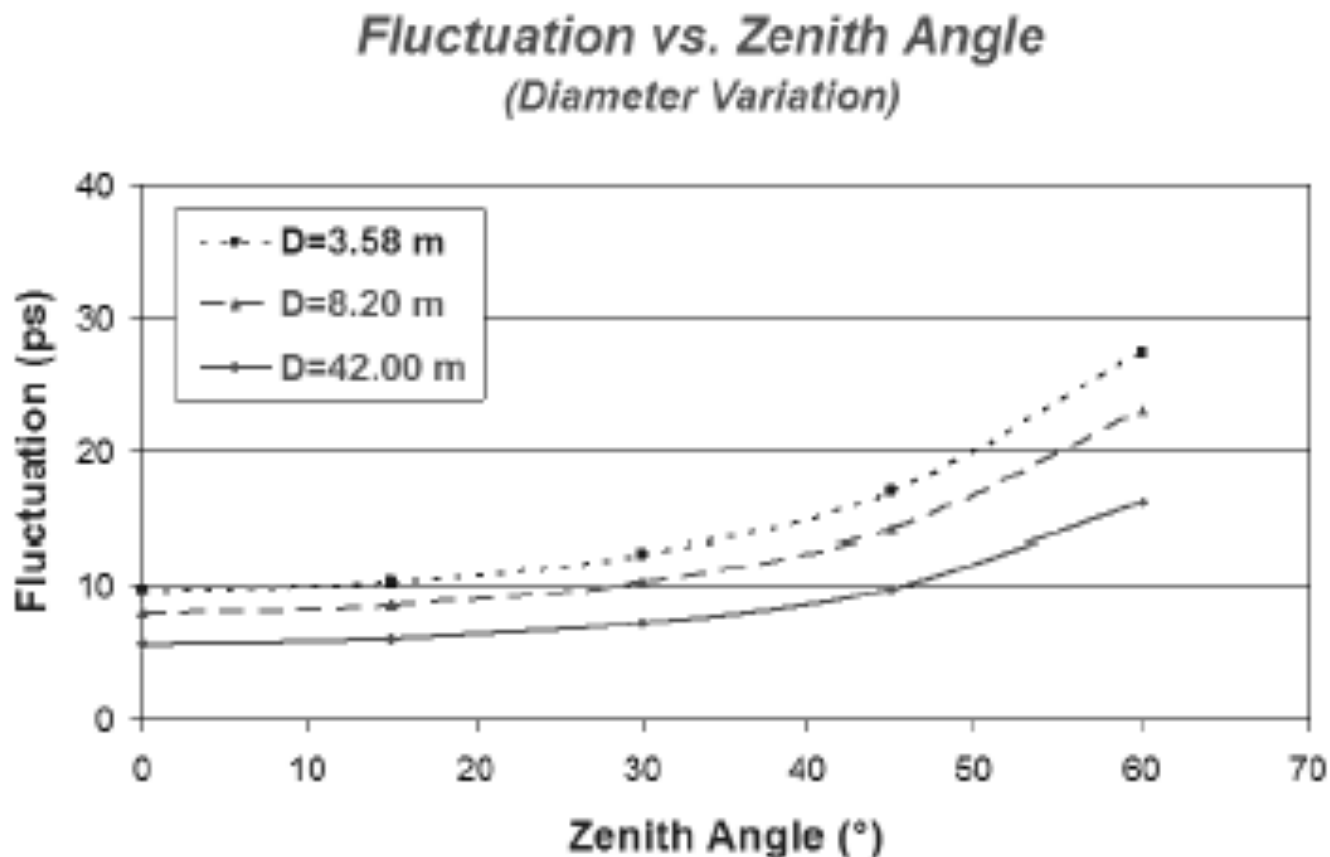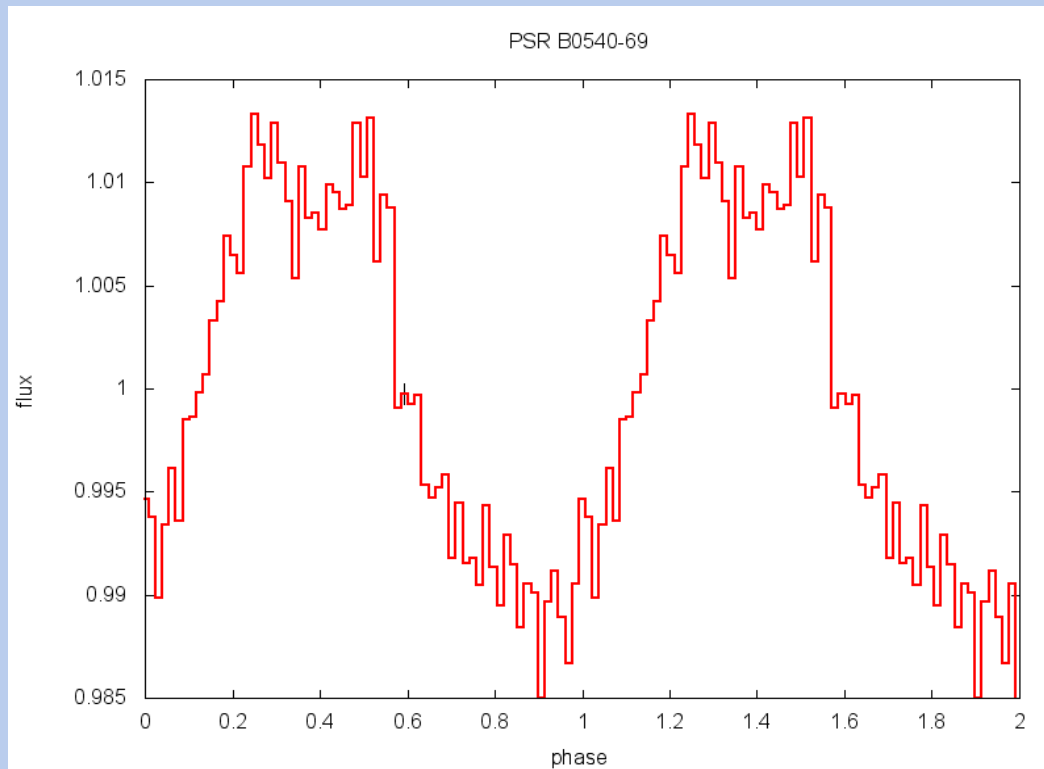
Atmospheric delay

Figure 4. Delay time fluctuation as a function of the telescope diameter and the Zenith angle variation ($\lambda = 0.632\mu m$, $r_0 = 15cm$). The simulation compares La Silla (NTT), Paranal (VLT) and Armazones (ELT).

The second brightest pulsar: B0540-69 in the Large Magellanic Cloud

PSR B0540-69

**The braking index over 27 years of observations
is n = 2.087 +/- 0.013,
decidedly lower than the magnetic dipole value.**

This pulsar is approximately 100 time fainter than Crab's, therefore individual pulses cannot be detected.
In 2 hours of photon counting we extended by 9 years the time span over which optical data have been obtained and derived **the best light curve available in the literature.**

The faintest pulsar: Vela

(a)

(b) 1977 DATA

(c) 1979 DATA

Manchester et al.

Optical

0   **Gouiffes**   0.5
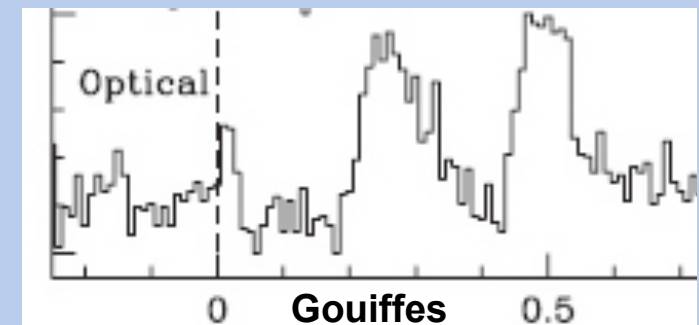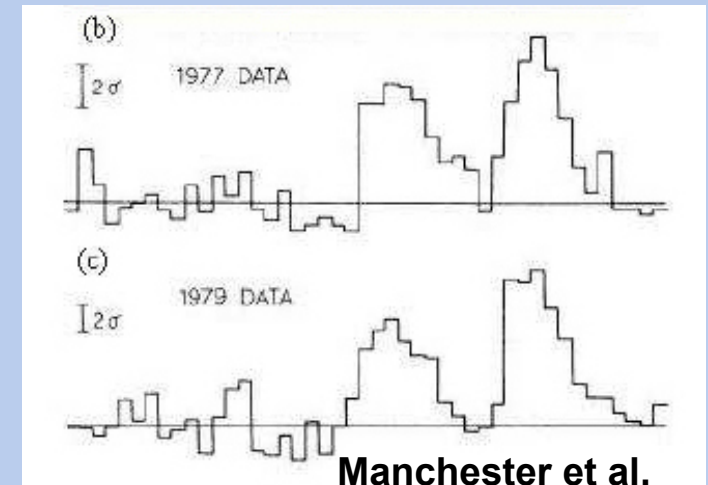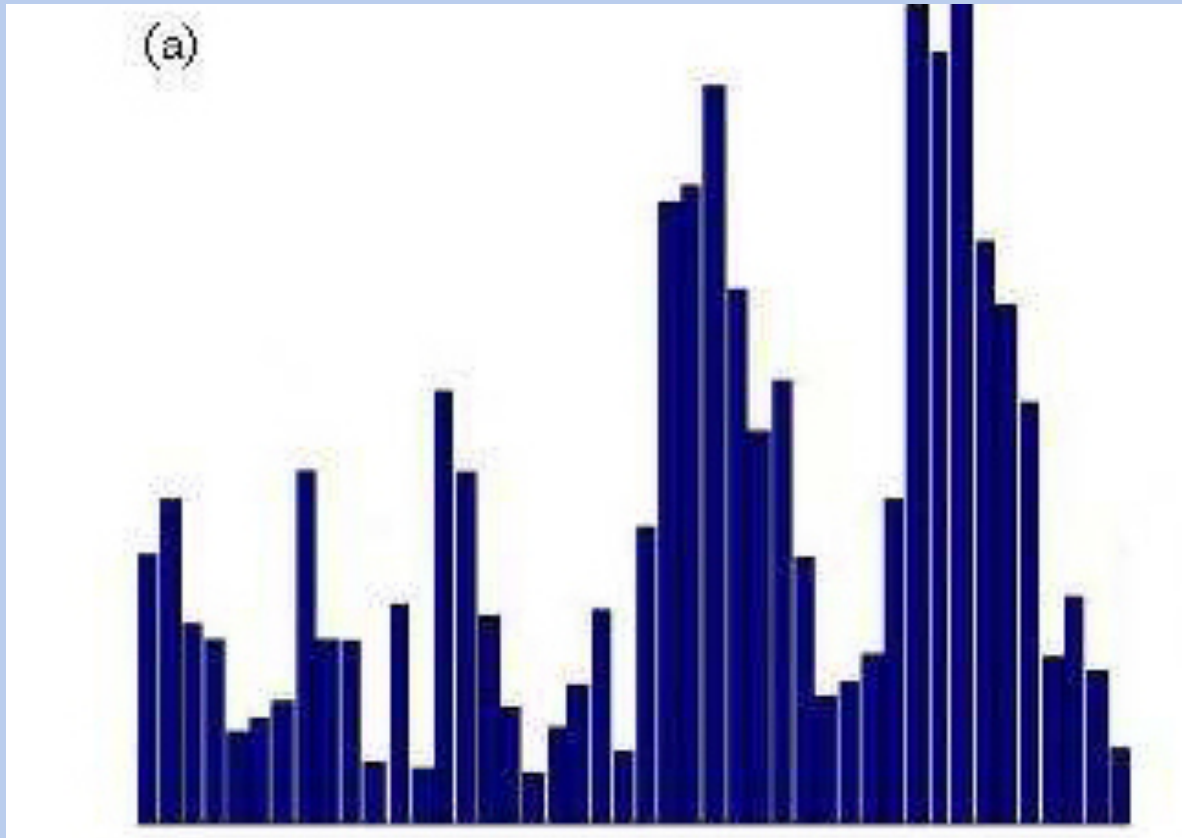
Vela's pulsar (period around 80 ms) is 10 times fainter than B0540-69.
The periodic signal is plainly evident from the Fourier transform.

The light curve (1 cycle shown), again one of the best in the literature, has a very complex shape.

Conclusions

AquEYE and IquEYE have proven the validity of our design and realization. The tests at two telescopes show that the instrument performs very well as extremely fast photon counter/ photometer. Reliability has been 100% both in Asiago and at NTT.

The concept is very modular, and can be easily adapted to any telescope.

With telescopes of modest size (< 4 m diameter) it is not possible to achieve significant results on quantum effects.
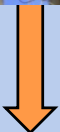
However, several high time resolution astrophysical problems (pulsars, gamma ray bursts, flickering and flare stars, cataclysmic variables, lunar and stellar occultations, and so on) can be investigated better than with other photometers, thanks to the fair quantum efficiency and superior time tagging capability.

Future: from Asiago and NTT to VLT ?

2008 Asiago
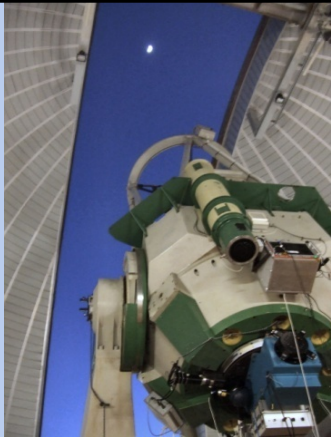
- The next step could be to realize an upgraded version of this instrument to be brought to the Very Large Telescope in early 2012. With VLT, we'll drastically improve the 'classical' capabilities of the instrument, and we'll start to have a glimpse of more complex 'quantum' observations.

2012? 1 VLT
2013? 2 VLTs: HBTII

2009-2010 NTT

HBTII with VLT

Minimum mirror diameter to achieve S/N=3 with 1h 2h 3h at 5400A

QE=0.4
Bandwidth 10^{10} Hz

(axis label) Apparent magnitude of the faintest star

(axis label) Mirror diameter (m)

VLT

LBT

MAGIC
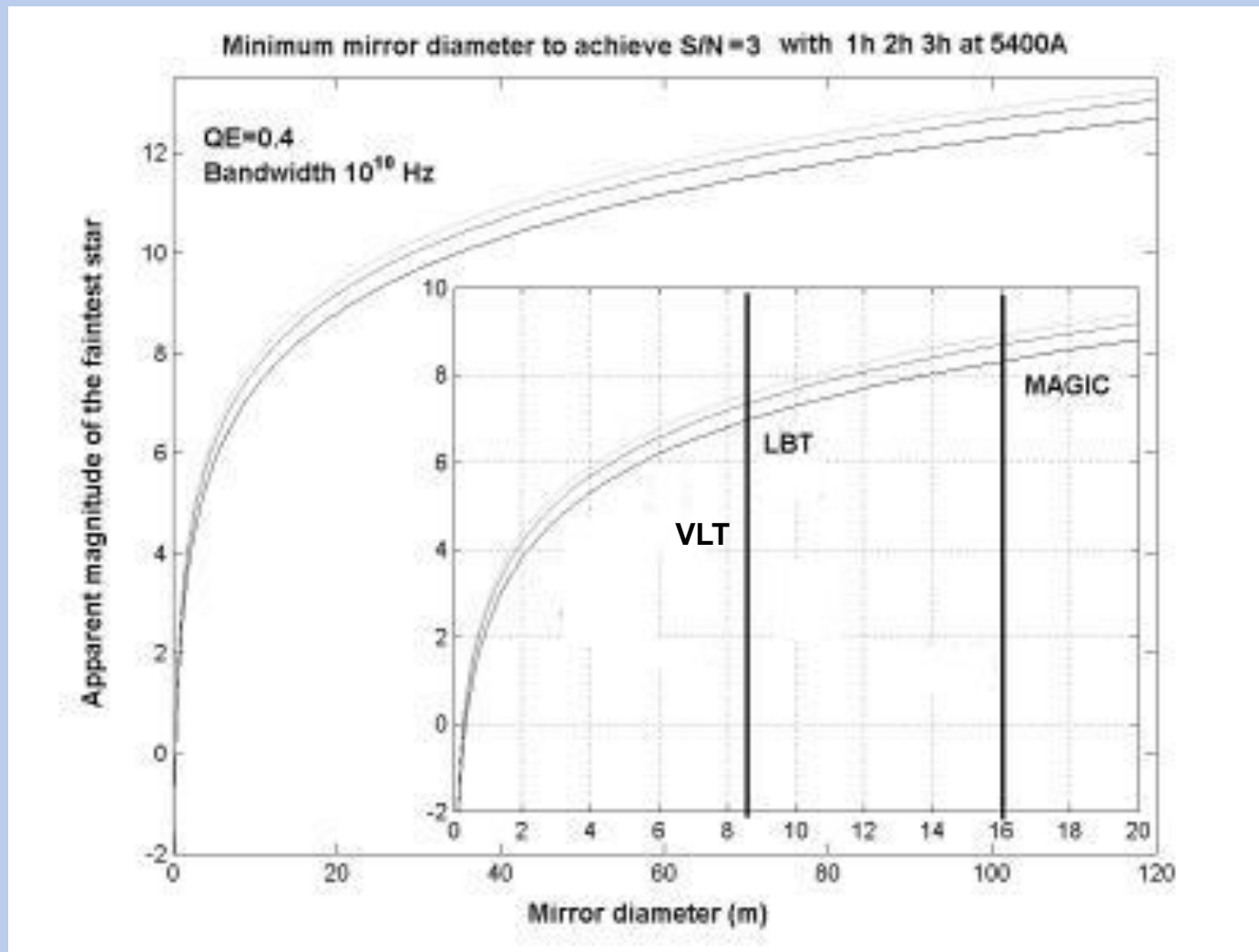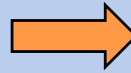
Futuristic: from VLT to E-ELT?

2012? 1 VLT
2013?2 VLTs: HBTII

2020? E-ELT: Quantum Astronomy

E-ELT – VLT: an exciting realization of HBTII

Paranal and Armazones are 22km apart, in an almost E-W configuration. The rotation of the Earth will perform the synthesis, pushing the angular scale by 100x from VLTI (200m).

A possible result E-ELT – VLT HBTII
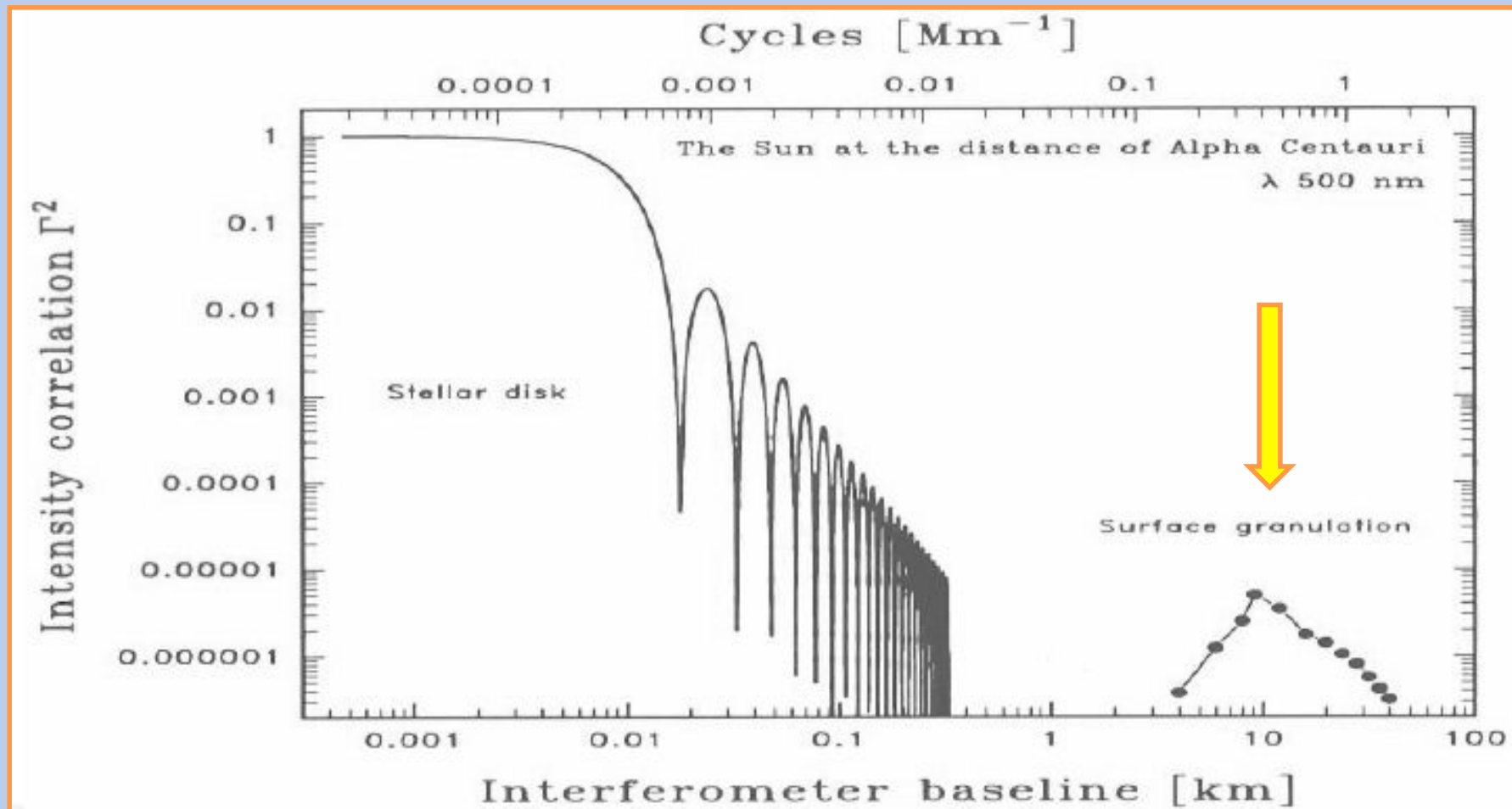
A final word on time

Time definition and determination should became again a major duty of Astronomy, as it was in the past.

If at all possible, the E-ELT should contain a primary time laboratory, of the same quality at NIST or USNO.

Thank you!

The Photon Orbital Angular Momentum

Among the properties of light still poorly exploited in Astronomy, **is the Orbital Angular Momentum (OAM) and associated Optical Vorticity (OV)**.

OAM has many interesting properties in the radio domain, e.g. for interstellar or interplanetary plasma physics diagnostic or for radio interferometry from the Moon or even for rotating Black Holes (M. Harwit, 2003, B. Thidé et al., 2007, F. Tamburini and B. Thidé, 2011).

It can also be used in the optical domain for coronagraphic applications.

Total EM field Angular Momentum

Electromagnetic (EM) beams do not only carry energy, power (Poynting flux, linear momentum), and spin angular momentum (SAM, wave polarization), but also *orbital angular momentum* (OAM).

The total angular momentum J^{EM} can be separated into two parts [*van Enk & Nienhuis*, 1992]:

$$\mathbf{J}^{EM} = \frac{1}{2iT} \left\{ \oint \oint \ast \, dd \quad xx \quad \varsigma \quad _{iii}\left(\oplus \quad _0 \right) \quad \right) \quad \hat{} \quad \right\}$$

the first part is the *spin angular momentum* **(SAM) S^{EM}** *, a.k.a. **wave polarization**,

the second part is the **orbital angular momentum (OAM) L^{EM}**.

In general, **both linear momentum P^{EM}**, *and* **angular momentum J^{EM} = S^{EM} + L^{EM} are radiated all the way out to the far zone (**see e.g. *Jackson, Classical Electrodynamics***).**

EM Angular Momentum postulated by Poynting already in 1909

Proc. Roy. Soc. London

The Wave Motion of a Revolving Shaft, and a Suggestion as to the Angular Momentum in a Beam of Circularly Polarised Light.

By J. H. POYNTING, Sc.D., F.R.S.

(Received June 2,—Read June 24, 1909.)

The analogy between circularly polarised light and the mechanical model suggests that a similar relation between torque and energy may hold in a beam of such light incident normally on an absorbing surface. If so, a beam of wave-length λ containing energy E per unit volume will give up angular momentum $E\lambda/2\pi$ per second per unit area. But in the case of light waves $E = P$, where P is the pressure exerted. We may therefore put the angular momentum delivered to unit area per second as

$$P\lambda/2\pi.$$

Two recent papers

Light with a twist in its tail

Miles Padgett and L. Allen

Contemporary Physics (2000) vol. 41, nr.5, pag. 275-285

Twisted photons, by G. Molina-Terriza, J. Torres and L. Torner

The orbital angular momentum of light represents a fundamentally new optical degree of freedom. Unlike linear momentum, or spin angular momentum, which is associated with the polarization of light, orbital angular momentum arises as a subtler and more complex consequence of the spatial distribution of the intensity and phase of an optical field - even down to the single photon limit. Consequently, researchers have only begun to appreciate its implications for our understanding of the many ways in which light and matter can interact, or its practical potential for quantum information applications. This article reviews some of the landmark advances in the study and use of the orbital angular momentum of photons, and in particular its potential for realizing high-dimensional quantum spaces.

SAM vs. OAM

- SAM is tied to the **helicity (polarization)** of the light beam and **for a single photon** its value is:

$$S_z = \pm (h/2\pi)$$

- OAM is tied to the **spatial structure of the wavefront:** the orbital terms are generated by the *gradient of the phase;* it determines the helicoidal shape of the wave front; **for a single photon** it assumes the value :

$$L_z = l \ (h/2\pi)$$

with l = 0 for a plane wave with **S || k**, and $l \neq 0$ for a helicoidal wave front because **S** precesses around **k**.

Polarization enables only **two photon spin states,** but actually photons can exhibit **multiple OAM eigenstates,** *allowing single photons to encode much more information .*

The mathematics of OAM

$$u_{pl}(r, \phi, z) = \frac{C}{(1 + z^2/z_R^2)^{1/2}} \left[\frac{r\sqrt{2}}{w(z)}\right]^l L_p^l\left[\frac{2r^2}{w^2(z)}\right] exp\left[\frac{-r^2}{w^2(z)}\right] \times$$

$$\times exp\left[\frac{-ikr^2 z}{2(z^2 + z_R^2)}\right] exp(-il\phi) exp\left[i(2p + l + 1) tan^{-1}\frac{z}{z_R}\right]$$

the mathematical representation in terms of Laguerre - Gauss modes contains two integer numbers:
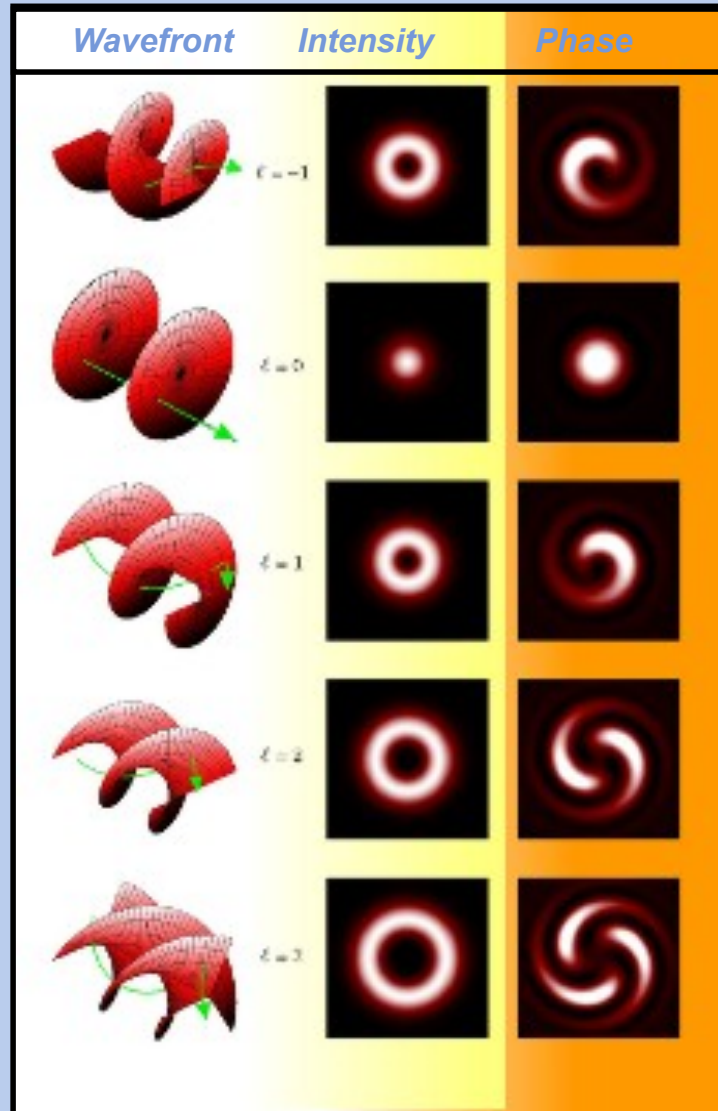
l = nr. of helicoidal twists along a wavelength, *p* = nr. of radial nodes

The red ovals underline the general terms applying also to non-laser beams. In the following we concentrate on *l* .

Graphical representation of L – G modes

The figure shows a graphical representation for $p = 0$.

l = topological charge

The wavefront has an helical shape composed by ℓ lobes disposed around the propagation axis *z*.

A phase singularity called *Optical Vortex* is nested inside the wavefront, along the axis z.

OPTICAL VORTICES OV

Another representation of the Optical Vortex:

helicoidal shape of the wavefront

⬇

indetermination of the phase on the axis around which the wavefront twists

⬇

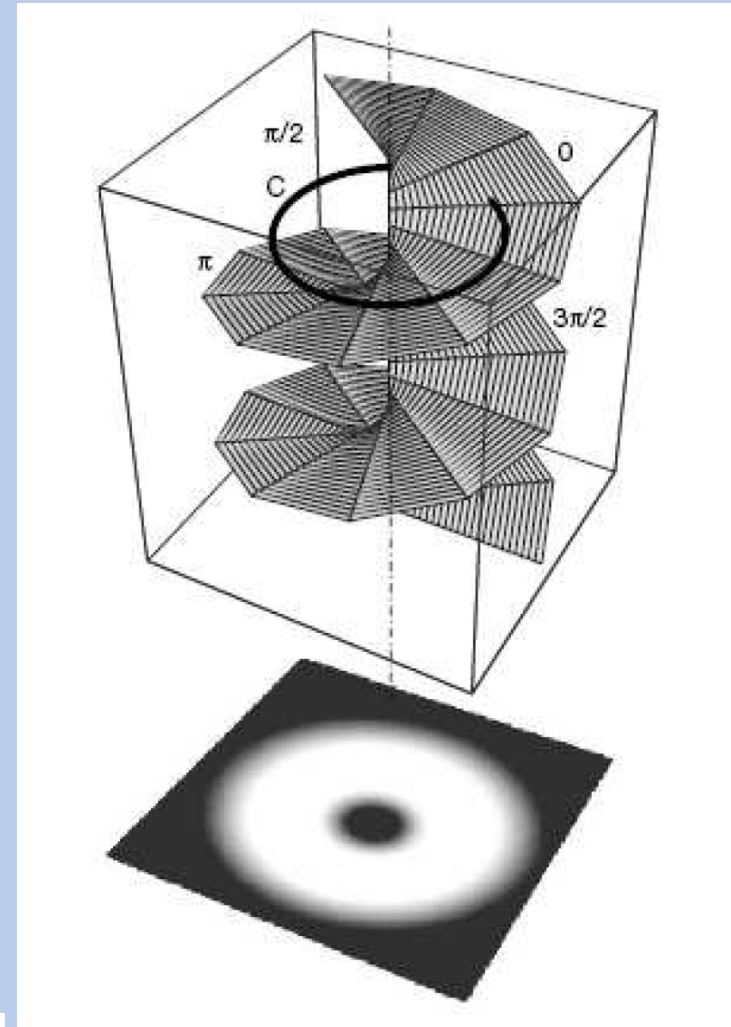**zero intensity of the field on such axis (destructive interference)**

⬇

Optical Vortex described by the topological *charge:*

$$Q = \frac{1}{2\pi} \oint_c \nabla\chi \cdot d\vec{s} \quad \Longleftrightarrow \quad Q = l$$

Example: OAM IN A LASER PARAXIAL BEAM
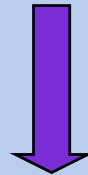
In a **PLANE** EM wave :

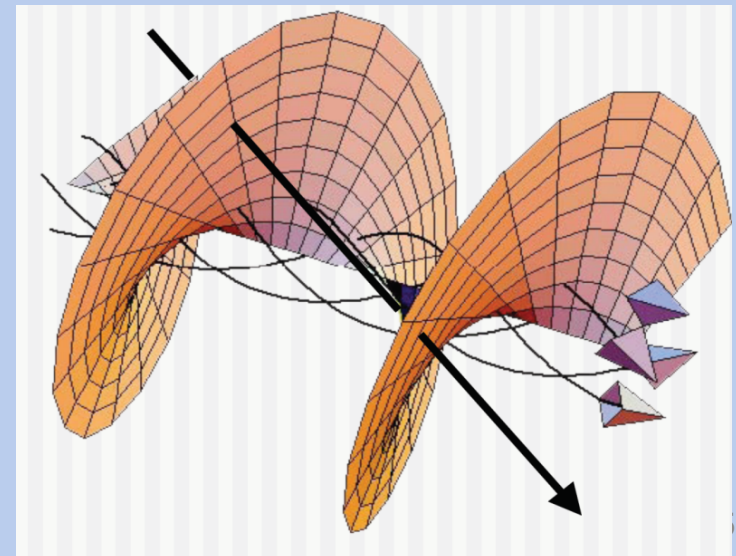$E_z = B_z = 0$, S is parallel to k ⟹ **J = 0**

In a **LASER** generated paraxial beam:

$E_z \neq 0$, $B_z \neq 0$, S is no longer parallel to k

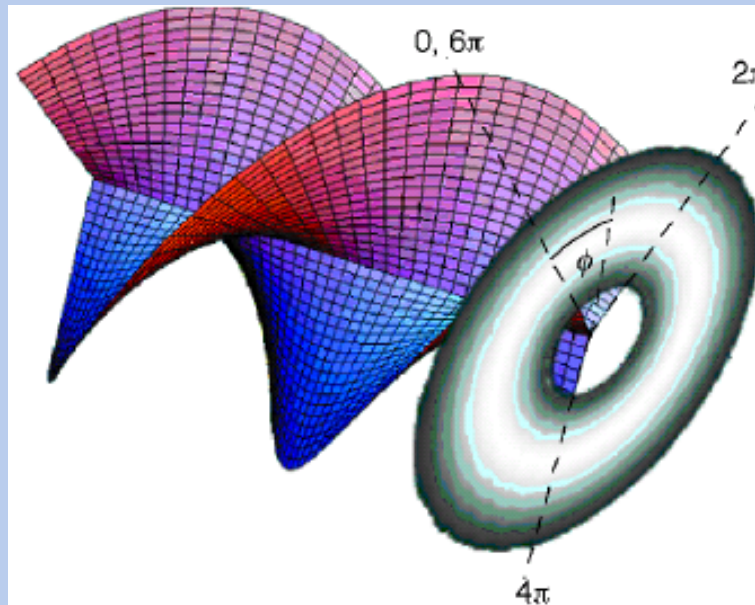⤷ S gets a radial plus an azimuthal component: ⟹ $J = J_z \neq 0$

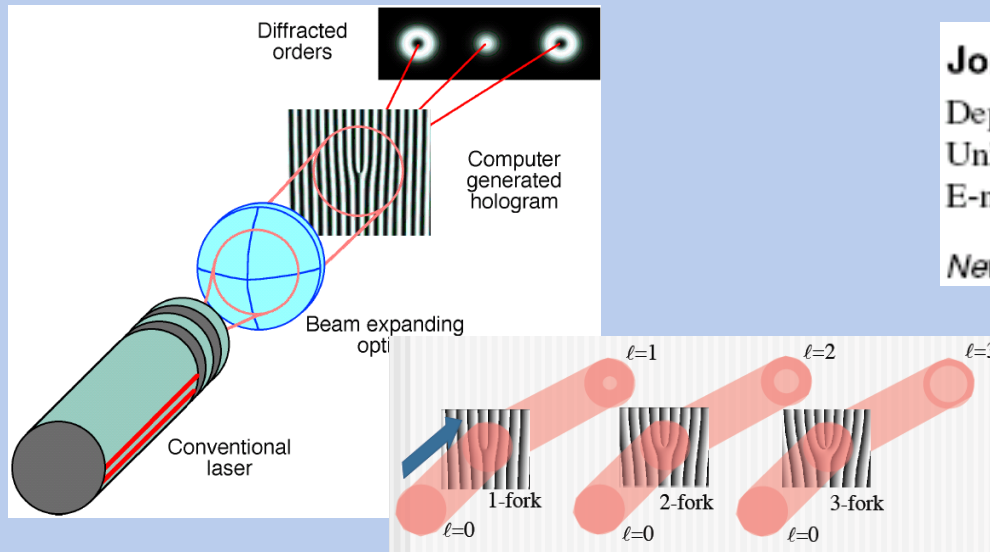Poynting's vector rotates around the average direction of propagation :

Imparting OAM onto a laser beam

The generation of beams carrying OAM proceeds thanks to the insertion in the optical path of *a phase modifying device* which imprints vorticity on the phase distribution of the incident beam.

Imparting OAM onto a laser beam with the help of a fork hologran or a spiral plate

Diffracted orders

Computer generated hologram

Beam expanding optics

Conventional laser

Jonathan Leach, Eric Yao and Miles J Padgett

Department of Physics and Astronomy, Kelvin Bld, University Ave, University of Glasgow, Glasgow G12 8QQ, UK

E-mail: j.leach@physics.gla.ac.uk

$\ell=1$ $\ell=2$ $\ell=3$

1-fork 2-fork 3-fork

$\ell=0$ $\ell=0$ $\ell=0$

(a) (b)

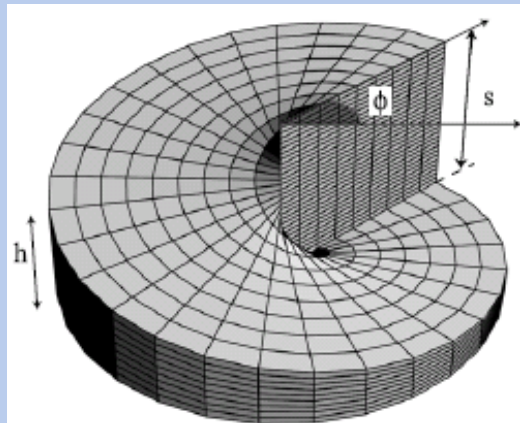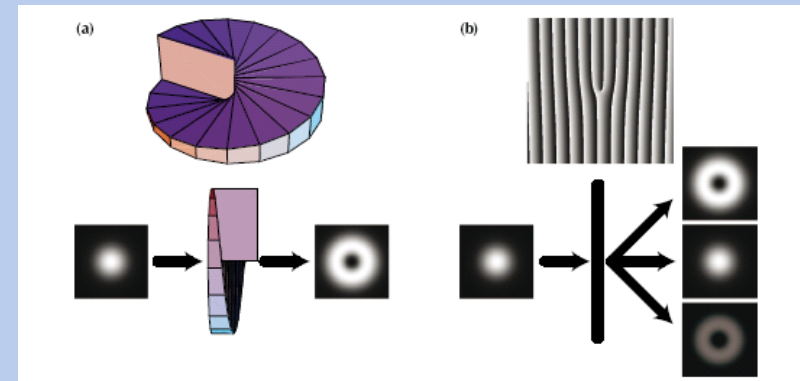**Figure 1.** A spiral phase plate of refractive index n. The thickness of the phase plate h is proportional to the azimuthal position given by ϕ.

Our results

Our first results with a *l* = 1 fork hologram:
1 - overcoming the Rayleigh limit in the laboratory

Overcoming the Rayleigh Criterion Limit with Optical Vortices

F. Tamburini, G. Anzolin, G. Umbriaco, A. Bianchini, and C. Barbieri

Department of Astronomy, University of Padova, vicolo dell' Osservatorio 2, Padova, Italy
(Received 12 June 2006; published 16 October 2006)

We experimentally and numerically tested the separability of two independent equally luminous monochromatic and white light sources at the diffraction limit, using optical vortices (OV). The diffraction pattern of one of the two sources crosses a fork hologram on its center generating the Laguerre-Gaussian (LG) transform of an Airy disk. The second source, crossing the fork hologram in positions different from the optical center, generates nonsymmetric LG patterns. We formulated a criterion, based on the asymmetric intensity distribution of the superposed LG patterns so created, to resolve the two sources at angular distances much below the Rayleigh criterion. Analogous experiments in white light allow angular resolutions which are still one order of magnitude below the Rayleigh criterion. The use of OVs might offer new applications for stellar separation in future space experiments.

Our first results with a $l = 1$ fork hologram:
2 – Producing Optical Vortices with starlight
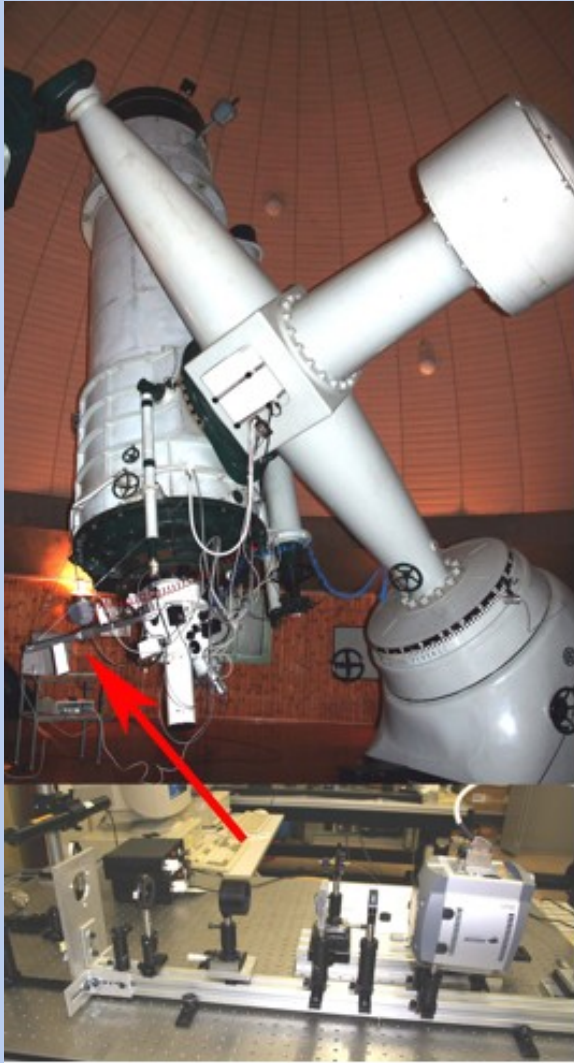
**Optical vortices with starlight
G. Anzolin, F. Tamburini, A. Bianchini, G. Umbriaco, and C. Barbieri
(2008, Astron. & Astrophys.)**

The previously described device with a $l = 1$ fork hologram was taken to the 122 cm Asiago telescope.

Real star images were fed to the optical train.

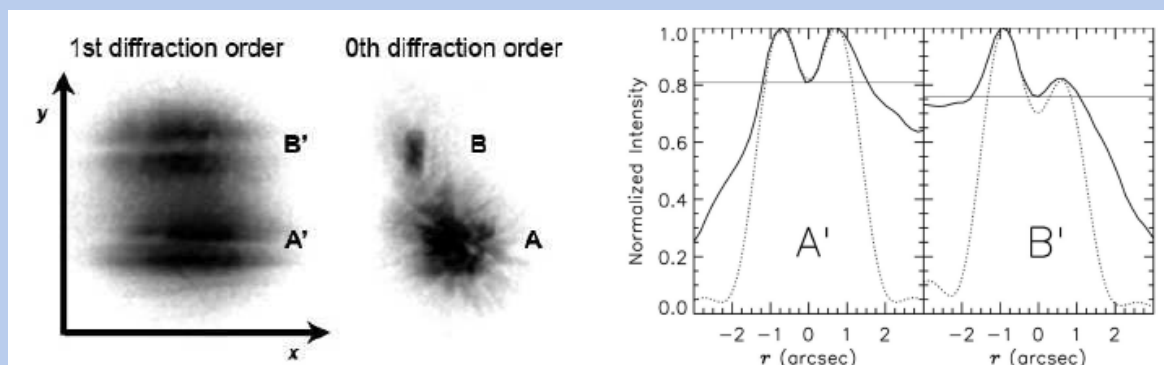# A poor-man solution to seeing problems: lucky imaging

Fig. 3. Image (right) and dispersed OVs (left) of α Her A and B obtained by adding the selected best frames (see text). Intensities are displayed in a squared greyscale. The OV profiles were taken along the y axis, perpendicular to the direction of dispersion x.

Fig. 5. Profiles of the OVs generated by α Her A (A', left panel) and α Her B (B', right panel) extracted along the y axis of Fig. 3. Dotted lines represent the numerical simulations of ℓ = 1 chromatically dispersed OVs generated by a pupil with a circular 7% obstruction. Thin solid lines indicate the intensity value at the central dips of the observed
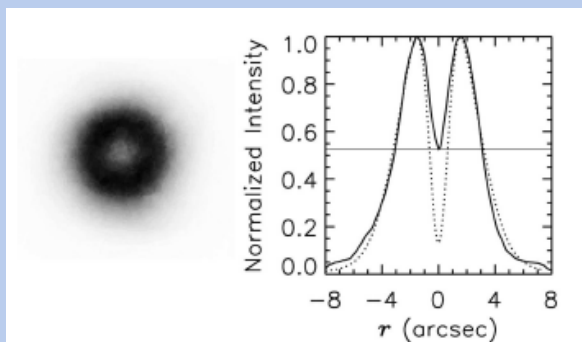
Fig. 6. Left: the narrow-band OV of α Boo obtained by summing the selected frames (see text). The intensity is displayed in a squared greyscale. Right: profile of the OV across the direction perpendicular to the dispersion (solid line). The dotted line represents the numerical simulation of an ℓ = 1 OV produced by a PSF modelled as described in the text, with a spectral range of 300 Å. The thin solid line indicates the observed intensity in the central dark region.

This fairly old telescope does not possess an AdOpt device, so we had to take very short exposures and select the best frames.

Nevertheless we could convincingly obtain OVs with single and double stars.
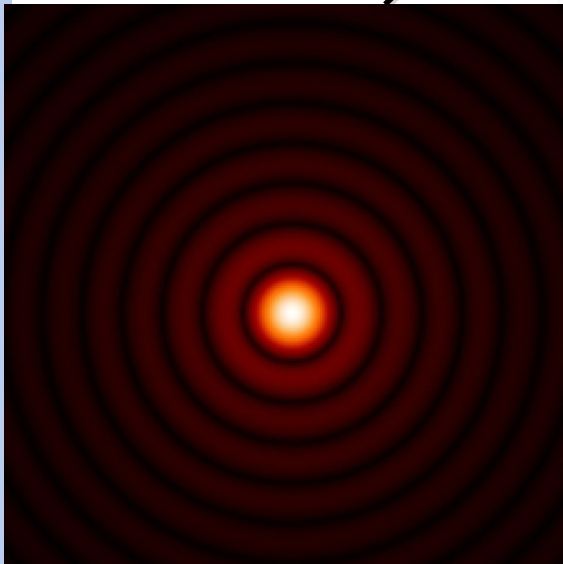
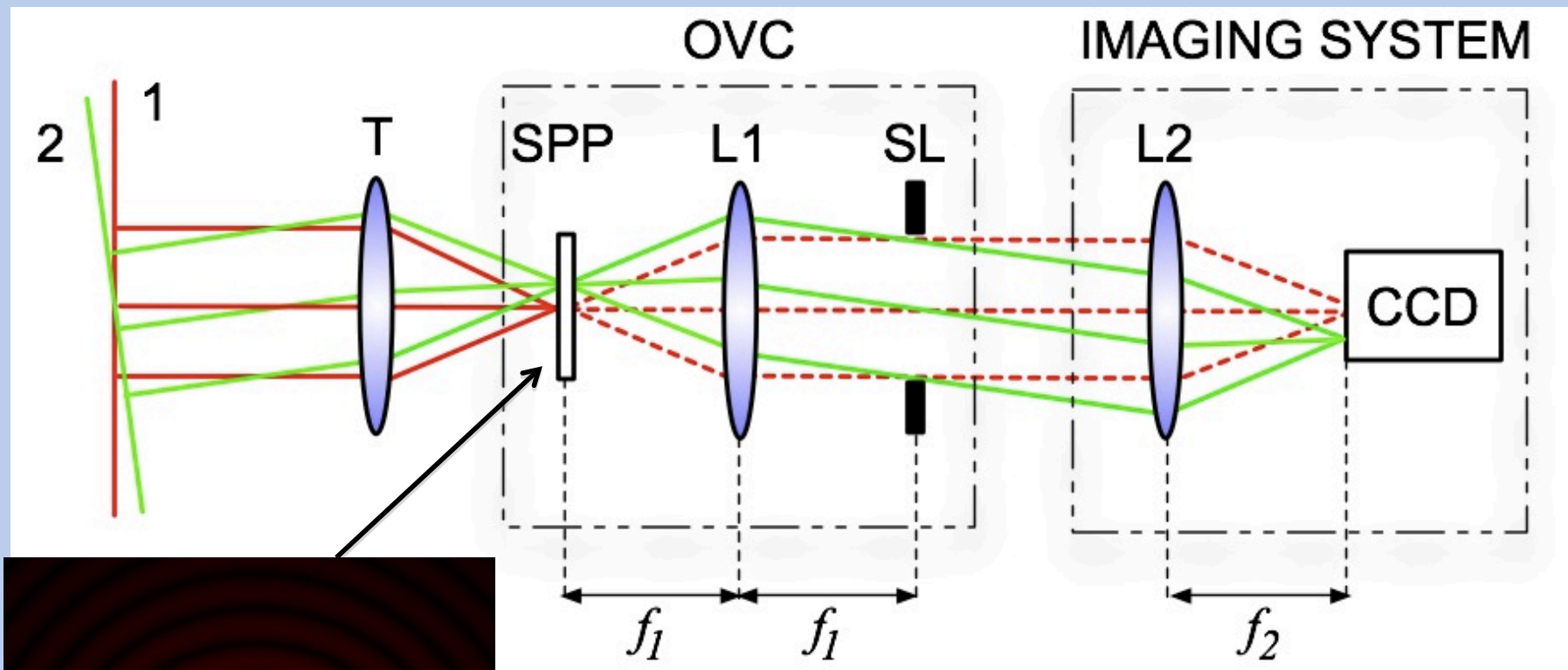# 3 - OVs for astronomical coronagraphy

OVs for Coronagraphy
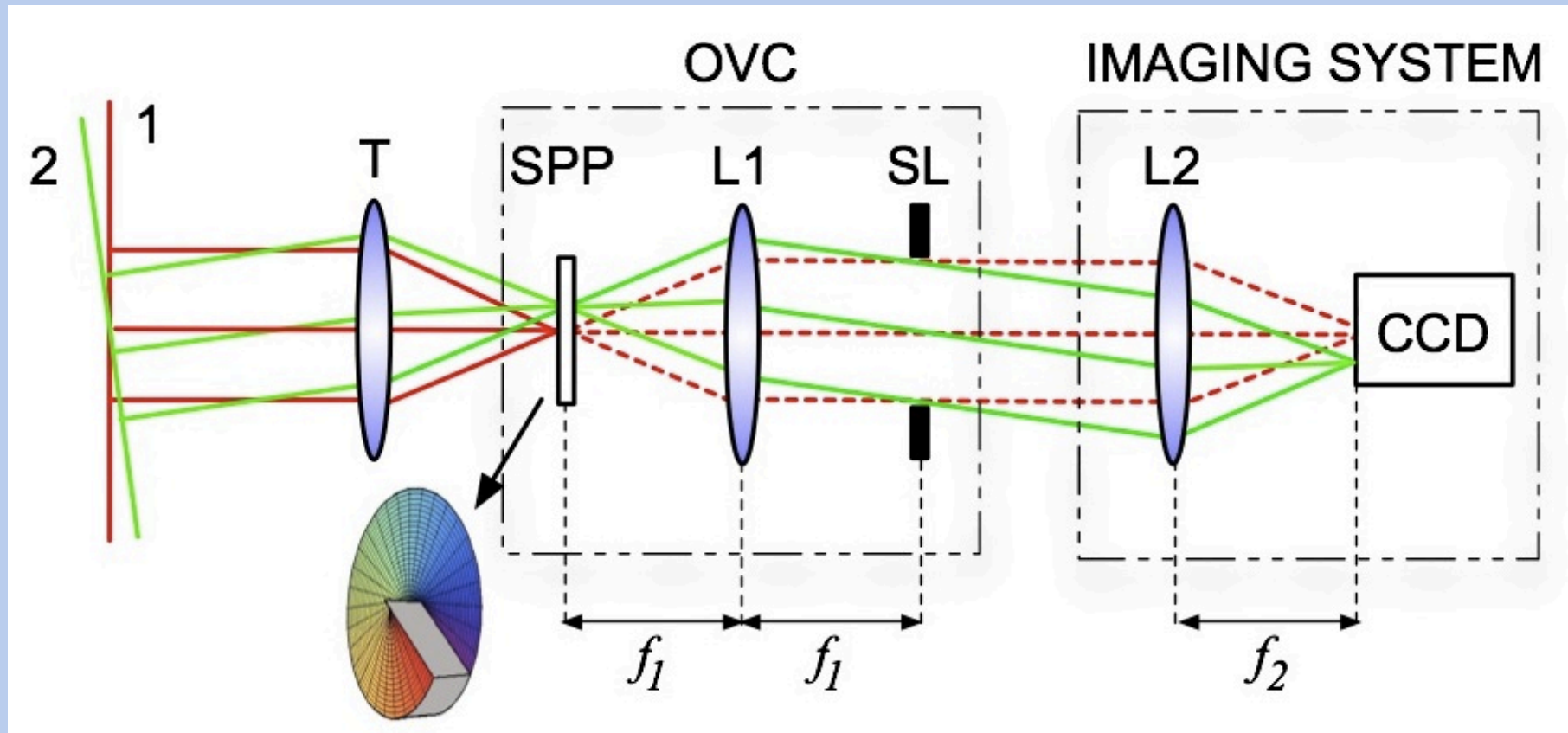
Phase mask placed in the telescope focal plane. It generates a $\ell = 2$ (more generally, with an even charge) OV.
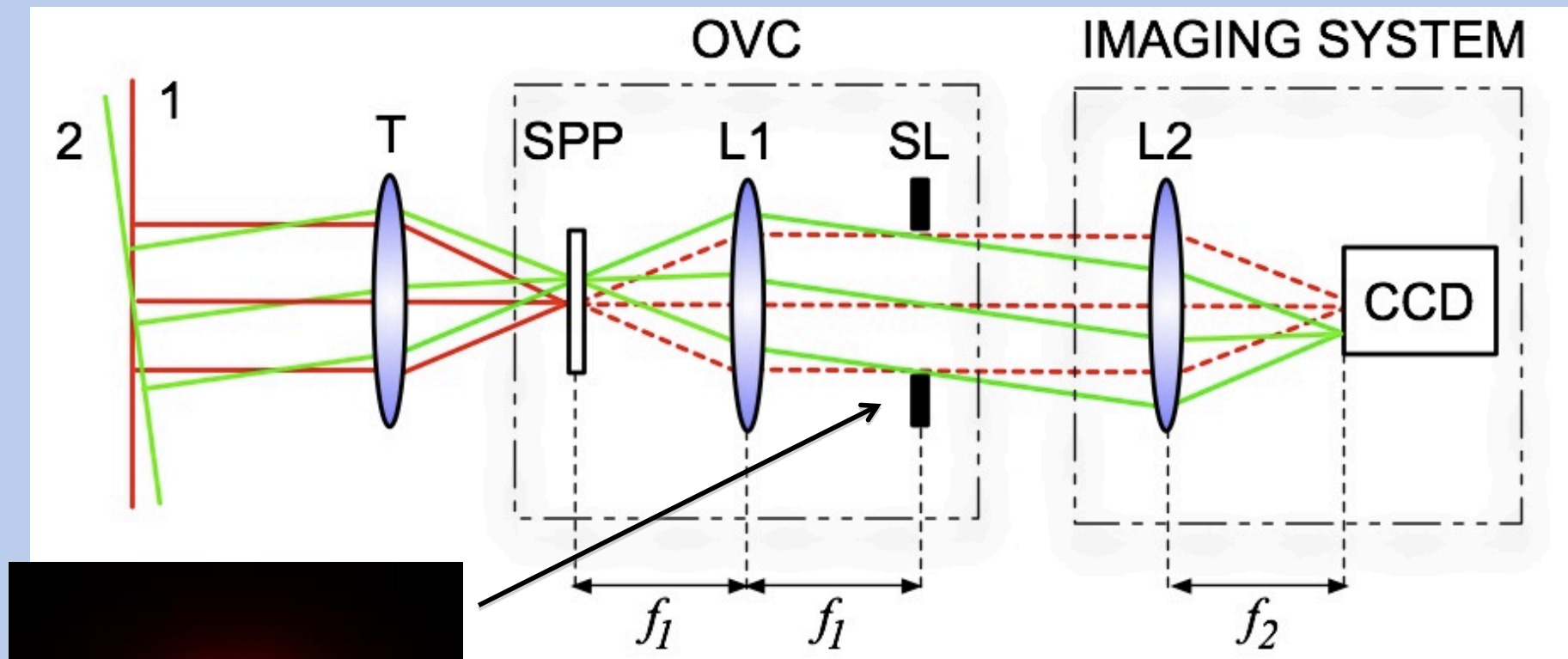**Consider two stars in a close binary system: the off-axis secondary star will pass through the Lyot mask, while the ring of the primary is blocked.**
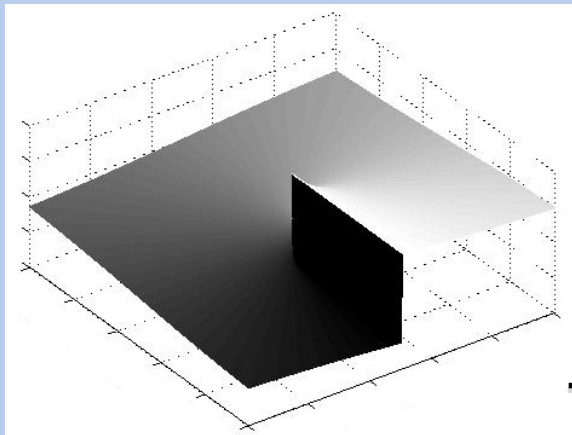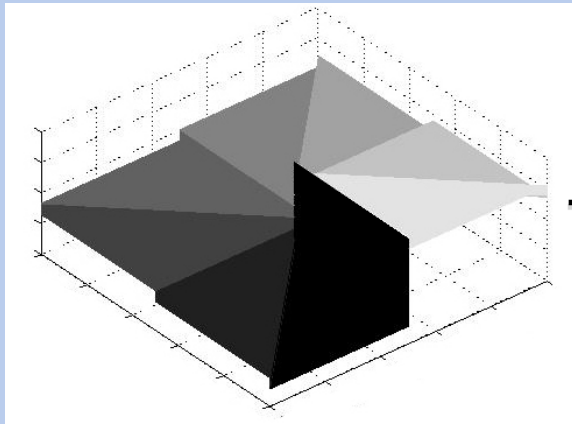
OVs for Coronagraphy

Incident Airy diffraction pattern that crosses the optical singularity of the SPP

OVs for Coronagraphy

**Optical vortex then blocked by
a circular aperture called Lyot stop**

N steps	Fainting	λ_{min}
8	$2.27 \cdot 10^{-4}$	624
16	$6.70 \cdot 10^{-5}$	585
32	$1.75 \cdot 10^{-5}$	567
64	$4.42 \cdot 10^{-6}$	558
128	$1.09 \cdot 10^{-6}$	554
512	$7.21 \cdot 10^{-8}$	551
∞	$5.63 \cdot 10^{-10}$	550

With an ideal spiral phase mask the achieved contrast is sufficient for the direct detection of extra-solar planets!

Our work on *l* = 2 Spiral Phase Plates: fabricating our own masks

Several *l* = 2 masks have been already fabricated with nanotechnologies on PMMA plates by our group, both at the TASC-LILIT facility in Trieste and at the University of Singapore. More recently a new Nanotech Lab with better machinery has been dedicated at the University of Padova.

M. Prasciolu [a,*], F. Tamburini [b], G. Anzolin [b], E. Mari [b], M. Melli [c], A. Carpentiero [a], C. Barbieri [b], F. Romanato [a,d,e]
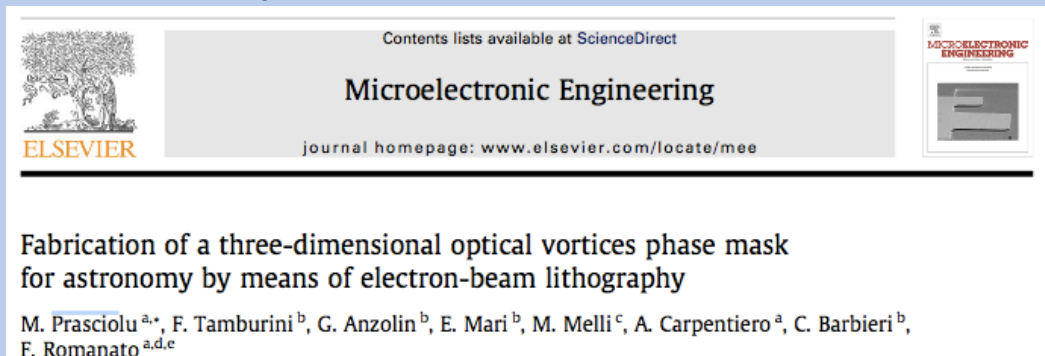
These masks have been implemented in a coronagraphic device for the 122-cm telescope.

Fabrication and Testing of *l=2* Optical Vortex phase masks for Coronography

Elettra Mari,[1,*] Gabriele Anzolin,[2] Fabrizio Tamburini,[3] Mauro Prasciolu,[4] Gabriele Umbriaco,[3] Antonio Bianchini,[3] Cesare Barbieri,[3] and Filippo Romanato,[4,5,6]

[1]CISAS "G.Colombo", University of Padua, Via Venezia 15 35131, Padova, Italy
[2]ICFO - Institut de Ciénces Fotòniques, Mediterranean Technology Park, Av. del Canal Olimpic 08860 Castelldefels (Barcelona), Spain
[3]Department of Astronomy, University of Padua, Vicolo dell'Osservatorio 3, 35122 Padova, Italy
[4]CNR-INFM TASC National Laboratory, S.S.14 Km 163.5, Area Science Park, 34012 Basovizza, Trieste, Italy
[5]Department of Physics, University of Padua, Via F. Marzolo 8, 35131 Padova, Italy
[6]LaNN, Laboratory for Nanofabrication of Nanodevices, Veneto Nanotech, Via San Crispino 106, 35129 Padova, Italy

Coronagraphic tests at Asiago 122cm Galileo telescope

Epsilon lyrae 2 | SPP on eps Lyr C | SPP on eps Lyr D
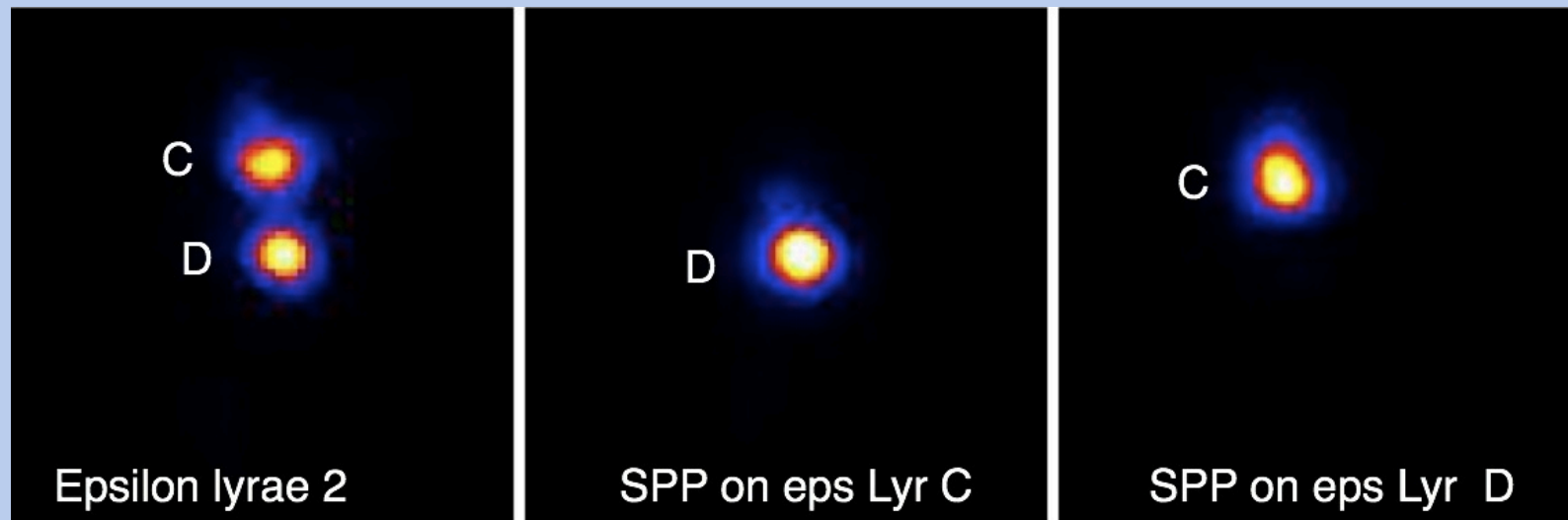
We obtain (no adopt, only lucky imaging), almost two orders of magnitude of fainting.
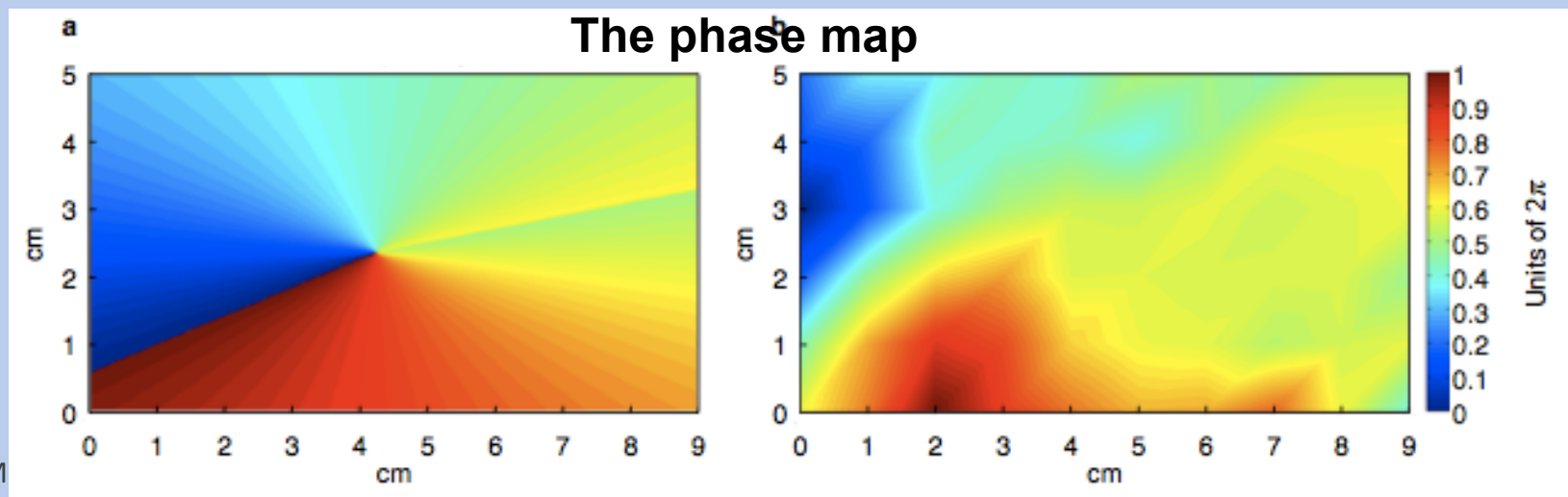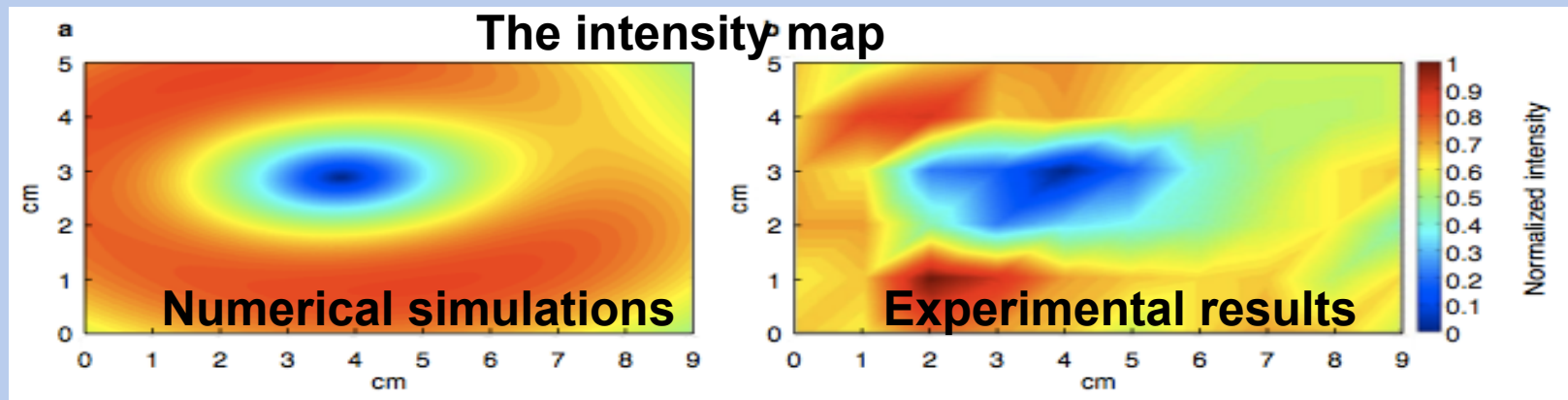
Demonstration of an optical vortex coronagraph at the 122 cm Asiago telescope

E. Mari[1], F. Tamburini[2], G. Umbriaco[2], F. Romanato[3,4,5], G. A. Swartzlander Jr[6], Bo Thidé[7], C. Barbieri[1,2], and A. Bianchini[2]
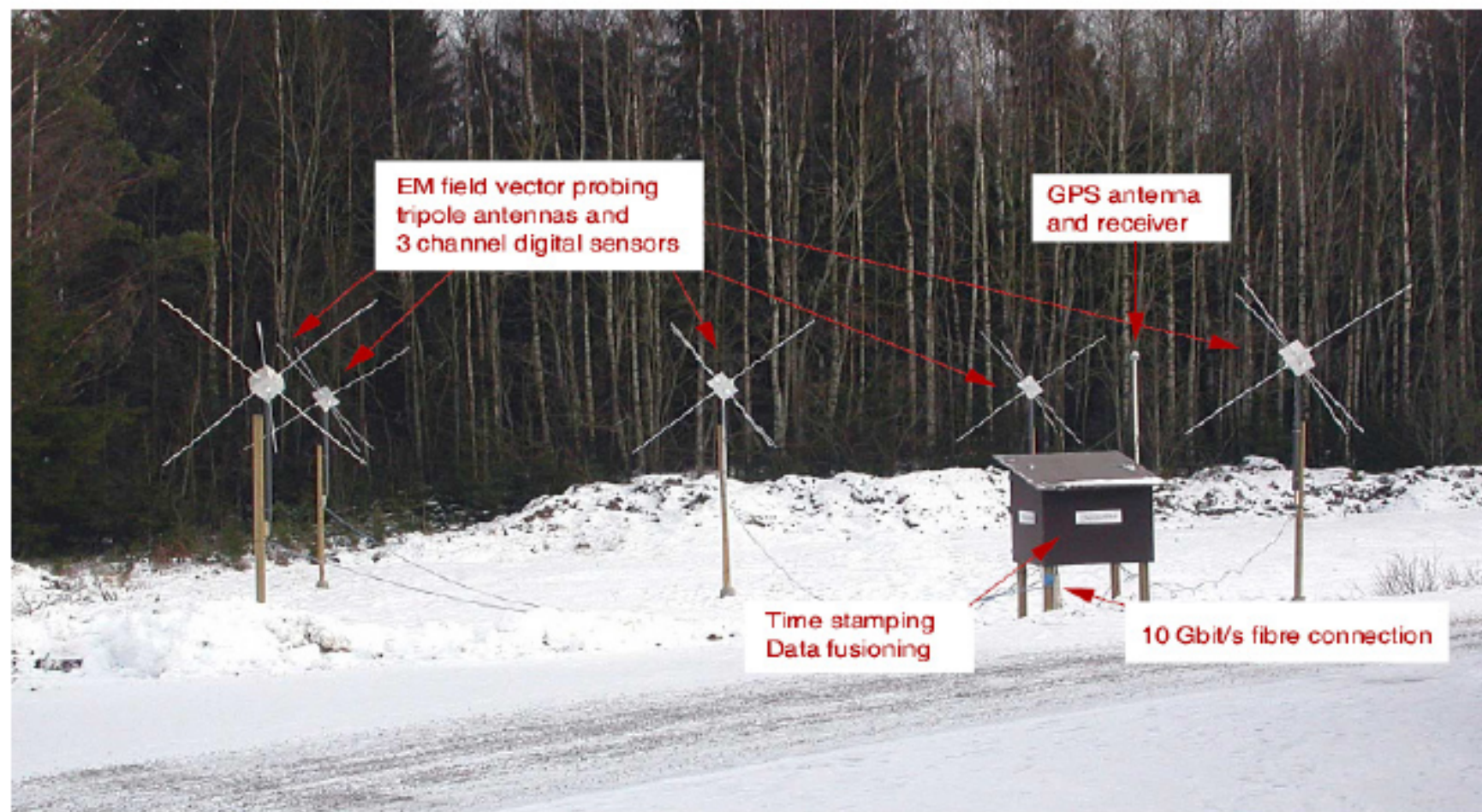
Being submitted to A&A

Radio Applications

We applied our knowledge of the OAM to the radio domain. We have shown experimentally (in the anechoic chamber of Uppsala University) how OAM and vorticity can be readily imparted onto *radio beams*. The frequency was 1.4 GHz

The intensity map — Numerical simulations / Experimental results

The phase map

LOIS Test Station, the Risinge site, Växjö, Sweden

EM field vector probing tripole antennas and 3 channel digital sensors

GPS antenna and receiver

Time stamping Data fusioning

10 Gbit/s fibre connection

This opens the possibility to work with OAM at frequencies low enough to allow the use of antennas and digital signal processing.